The Lyme Disease agent co-opts adiponectin receptor-mediated signaling in its arthropod vector

Xiaotian Tang,[1,*, †] Yongguo Cao,[1,2,*] Gunjan Arora,[1] Jesse Hwang,[1] Andaleeb Sajid,[1] Courtney L. Brown,[3] Sameet Mehta,[4] Alejandro Marín-López,[1] Yu-Min Chuang,[1] Ming-Jie Wu,[1] Hongwei Ma,[1,5] Utpal Pal,[6] Sukanya Narasimhan,[1] and Erol Fikrig[1,†]

[1] Section of Infectious Diseases, Department of Internal Medicine, School of Medicine, Yale University, New Haven, CT, USA

[2] Department of Clinical Veterinary Medicine, and Key Laboratory for Zoonosis Research, Ministry of Education, College of Veterinary Medicine, Jilin University, Changchun, China

[3] Yale Combined Program in the Biological and Biomedical Sciences, Yale University, New Haven, CT, USA

[4] Yale Center for Genome Analysis, Yale University, New Haven, CT, USA

[5] Department of Microbiology, School of Basic Medicine, Fourth Military Medical University, Xi'an, Shaanxi, China

[6] Department of Veterinary Medicine, University of Maryland, College Park, Maryland, USA

*These authors contributed equally to the manuscript

[†]Corresponding authors: Erol Fikrig, Section of Infectious Diseases, Department of Internal Medicine, Yale University School of Medicine, erol.fikrig@yale.edu;

Xiaotian Tang, xiaotian.tang@yale.edu

Abstract

Adiponectin-mediated pathways contribute to mammalian homeostasis; however, little is known about adiponectin and adiponectin receptor signaling in arthropods. In this study, we demonstrate that *Ixodes scapularis* ticks have an adiponectin receptor-like protein (ISARL) but lack adiponectin – suggesting activation by alternative pathways. *ISARL* expression is significantly upregulated in the tick gut after *Borrelia burgdorferi* infection suggesting that ISARL-signaling may be co-opted by the Lyme disease agent. Consistent with this, RNA interference (RNAi)-mediated silencing of *ISARL* significantly reduced the *B. burgdorferi* burden in the tick. RNA-seq-based transcriptomics and RNAi assays demonstrate that ISARL-mediated phospholipid metabolism by phosphatidylserine synthase I is associated with *B. burgdorferi* survival. Furthermore, the tick complement C1q-like protein 3 interacts with ISARL, and *B. burgdorferi* facilitates this process. This study identifies a new tick metabolic pathway that is connected to the life cycle of the Lyme disease spirochete.

Keywords: Adiponectin receptor; *Ixodes scapularis*; *Borrelia burgdorferi*; Phospholipid metabolism; C1q-like protein 3 protein

Significance Statement

Adiponectin binds to adiponectin receptors and participates in glucose and lipid metabolism in mammals. In this study, we found that ticks have an adiponectin receptor-like protein but lack adiponectin. Importantly, we demonstrated that the Lyme disease agent, *Borrelia burgdorferi*, takes advantage of the adiponectin receptor signaling pathway to establish infection in its arthropod vector, *Ixodes scapularis*. Our study sheds light on the understanding of *Borrelia*-tick interactions and provides insights into how a human infectious disease agent may evolve to manipulate host metabolism for its own benefits. Understanding this pathway may lead to new ways to interfere with the *Borrelia* life cycle, and this mechanism may be applicable to additional microbes that are transmitted by ticks, mosquitoes or other arthropods.

Introduction

Adiponectin, adipocyte complement related protein of 30 kDa (or Acrp30), plays important roles in the regulation of metabolism, insulin sensitivity, and inflammation across species (Kadowaki et al., 2006; Ouchi and Walsh, 2007; Yamauchi et al., 2002). Adiponectin mediates its actions mainly via binding adiponectin receptors with its globular C1q domain (Buechler et al., 2010; Yamauchi et al., 2002). Two adiponectin receptors, AdipoR1 and AdipoR2, have been identified in mammals (Yamauchi et al., 2003). AdipoR1 and R2 belong to a family of membrane receptors predicted to contain seven transmembrane domains with an internal N terminus and an external C terminus (Yamauchi et al., 2003). AdipoR1 has a higher binding affinity for the globular form of adiponectin, whereas AdipoR2 has a greater affinity for full length adiponectin (Yamauchi et al., 2003). Interestingly, AdipoR1 and AdipoR2 double-knockout mice have increased triglyceride levels, and exhibit insulin resistance, demonstrating that AdipoR1 and AdipoR2 regulate lipid and glucose homeostasis (Kadowaki et al., 2006; Yamauchi et al., 2007). In yeast, a homolog of mammalian adiponectin receptors, ORE20/PHO36, is involved in lipid and phosphate metabolism (Karpichev et al., 2002). PHO36, can also interact with a plant protein, osmotin, a homolog of mammalian adiponectin, thereby controlling apoptosis in yeast (Narasimhan et al., 2005). Adiponectin and adiponectin receptors in disease-transmitting arthropods have not been characterized. By utilizing the amino acid sequence homology search in other model arthropods, adiponectin was not identified from *Drosophila melanogaster*, however, an adiponectin receptor which regulates insulin secretion and controls glucose and lipid metabolism was characterized

(Kwak et al., 2013). In addition, Zhu et al. (2008) cloned an adiponectin-like receptor gene from the silk moth, *Bombyx mori*, and found that infection with *B. mori* nucleopolyhedrovirus significantly increased adiponectin receptor mRNA levels in the midgut of susceptible *B. mori*, suggesting an association with pathogen infectivity.

Ixodes scapularis, the black-legged tick, is an important vector of the Lyme disease agent, *Borrelia burgdorferi* (Estrada-Peña and Jongejan, 1999), which causes approximately 300,000 cases annually in the United States (Rosenberg et al., 2018). *B. burgdorferi* is acquired when larval or nymphal ticks feed on infected animals, and is transmitted by nymphs or adults to vertebrate hosts (Kurokawa et al., 2020). Lyme disease in humans manifests as a multisystem disorder of the skin and other organs (e.g., joints, heart, and nervous system), resulting in patients experiencing cardiac, neurological, and arthritic complications (Asch et al., 1994; Singh and Girschick, 2004). A human vaccine against Lyme disease was approved by the FDA but is not currently available (Steere et al., 1998). Targeting tick proteins has the potential to disrupt tick feeding and alter *B. burgdorferi* colonization or transmission (Kurokawa et al., 2020), thereby offering a new way to interfere with the life cycle of the Lyme disease spirochete.

In the present study, we demonstrate that an *I. scapularis* adiponectin receptor-like (ISARL) protein facilitates *B. burgdorferi* colonization of the tick. ISARL-mediated stimulation of *I. scapularis* metabolic pathways are associated with spirochete colonization, and a tick complement C1q-like protein 3 contributes to ISARL activation.

Results

Identification and characterization of an *I. scapularis* adiponectin receptor-like protein

As tick metabolism changes during pathogen colonization, and adiponectin-associated pathways mediate diverse metabolic activities, we examined the *I. scapularis* database for two of the prominent genes linked to this pathway. The available *I. scapularis* database (taxid:6945) in NCBI was searched with the genes for mammalian adiponectin and adiponectin receptors, and results with the human and mouse genes are shown. There were no tick genes with high homology to the genes for human and mouse adiponectin full-length sequences. Interestingly, there was an *I. scapularis* gene (GenBank number: XM_029975213) with substantial homology to the human and murine adiponectin receptors, which we designated *I. scapularis* adiponectin receptor-like (*ISARL*). The corresponding ISARL protein sequence (GenBank number: XP_029831073) was also identified. The full-length *ISARL* mRNA encoded a protein with 384 amino acid residues and 71% amino acid sequence similarity to both the human and mouse adiponectin receptor protein 1 and 2. It also has high similarity (87%) to homologs from insect species, including the *Drosophila melanogaster* adiponectin receptor (GenBank number: NP_732759) (Fig. S1). Structure prediction and hydrophobicity analysis indicated that ISARL has seven transmembrane (TM) domains (Fig. S2). Comparison of the amino acid sequences between vertebrate and invertebrate species revealed that the

124 predicted transmembrane regions are highly conserved, especially in the TM3 domain
125 (Fig. S1).
126
127 **Silencing *ISARL* reduces *B. burgdorferi* colonization by *I. scapularis* nymphs**
128
129 As *I. scapularis* lack an obvious adiponectin homolog, we examined whether
130 expression of *ISARL* could be stimulated in the feeding vector by allowing ticks to engorge
131 on mice, including uninfected and *B. burgdorferi*-infected animals. Interestingly a blood
132 meal containing *B. burgdorferi* resulted in significantly increased expression of *ISARL* in
133 the nymphal tick guts ($P < 0.0001$) (Fig. 1A). This suggests that the presence of *B.*
134 *burgdorferi* in the blood meal helps to stimulate tick metabolic activity and/or that ISARL
135 may have an important role during *B. burgdorferi* colonization of the tick gut.
136
137 Since *ISARL* expression was upregulated upon *B. burgdorferi* infection**,** we
138 hypothesized that RNAi-mediated silencing of *ISARL* would affect *B. burgdorferi*
139 colonization by nymphal *I. scapularis*. To this end, *ISARL* or *GFP* (control) dsRNA was
140 injected into the guts of pathogen-free nymphs by anal pore injection. Then, the ticks were
141 allowed to feed on *B. burgdorferi*-infected mice. Quantitative RT-PCR (qPCR) analysis
142 showed a significant decrease of *ISARL* expression in the guts of ds *ISARL*-injected ticks
143 ($P < 0.01$) when compared to that in control ds *GFP*-injected tick guts (Fig. 1B), indicating
144 that the knockdown was successful. The engorgement weights of ds *ISARL*-injected
145 nymphs and control ds *GFP*-injected nymphs were comparable ($P > 0.05$) (Fig. 1C),
146 suggesting that silencing *ISARL* had no effect on tick feeding behavior. However, *ISARL*-

147 silenced nymph guts showed a marked reduction of the *B. burgdorferi* burden ($P < 0.001$)
148 when compared to that in control ticks (Fig. 1D), demonstrating that ISARL is associated
149 with *B. burgdorferi* colonization in the nymphal tick gut.
150
151 **Silencing *ISARL* does not affect *B. burgdorferi* transmission by *I. scapularis***
152 **nymphs**
153
154 To determine whether ISARL might also play a role in the transmission of *B.*
155 *burgdorferi* to the mammalian host, we silenced *ISARL* in *B. burgdorferi*-infected nymphs
156 by microinjection of ds *ISARL* into the ticks. The results showed that *B. burgdorferi*
157 burdens in the skin of mice (ear skin distal from the tick bite site) at 7, 14, and 21 days
158 post tick detachment, and in heart and joint tissues 21 days post tick detachment were
159 comparable ($P > 0.05$) in mice fed upon by ds *GFP*- or by ds *ISARL*-injected nymphs
160 (Figs. 1E and 1F), suggesting that silencing *ISARL* had no observable effect on *B.*
161 *burgdorferi* transmission by *I. scapularis* nymphs.
162
163 **Potential ISARL-dependent pathways associated with *B. burgdorferi* colonization**
164
165 To investigate the mechanisms underlying the association of ISARL with *B.*
166 *burgdorferi* colonization by *I. scapularis*, we assessed the presence or absence of ISARL
167 on tick physiology by comparing transcriptomes of ds *ISARL* and ds *GFP* (control)
168 injected ticks after engorgement on *B. burgdorferi*-infected or uninfected mice, using
169 RNA-seq.

After feeding on uninfected mice, 18 genes were significantly differentially expressed with six upregulated and 12 downregulated genes in the guts of ds *ISARL*-injected nymphal ticks when compared to that in control ds *GFP*-injected tick guts (Fig. 2A; Table S1). 35 genes were differentially expressed at a significant level, and all these genes were downregulated in the guts of ds *ISARL*-injected *I. scapularis* when compared to that in control ds *GFP*-injected ticks after feeding on *B. burgdorferi*-infected mice (Fig. 2B; Table S2). In addition, the transcriptome analysis further demonstrated that the *ISARL* gene was successfully silenced by RNAi (Tables S1 and S2) and this was also confirmed by qPCR (Fig. 2C). No common differentially expressed genes except *ISARL* were observed between control or experimental ticks feeding on uninfected or *B. burgdorferi*-infected mice (Fig. 2D), suggesting that the 34 significantly expressed genes were all induced by *B. burgdorferi,* or the influence of *B. burgdorferi* on the host blood components, rather than blood meal itself, in absence of ISARL.

In response to the blood meal, a significant change of the metabolic pathways in ticks was observed in absence of ISARL. In particular, based on GO functional classification and KEGG pathways analyses, the glutathione metabolic process with nine genes (e.g., gamma glutamyl transpeptidase, G2/mitotic-specific cyclin A, and glutathione S-transferase) was significantly altered. Moreover, the genes involved in metabolic pathways such propanoate metabolism and carbohydrate transport and metabolism (e.g., acyl-CoA synthetase and soluble maltase-glucoamylase) were also significantly changed in absence of ISARL after engorging on uninfected mice.

Similarly, many metabolism-associated genes, including multiple amino acids, lipids or sugars synthesis and transport genes (e.g., 3-hydroxyacyl-CoA dehydrogenase, glycogen phosphorylase, and sugar transporter) were significantly downregulated in the absence of ISARL after engorging on *B. burgdorferi*-infected mice. GO functional classification and KEGG pathways also showed that the most downregulated genes were involved in fatty acid, lipid and phospholipid, purine, amino acid, glycerophospholipid, and carbohydrate metabolism and transport pathways after silencing *ISARL* (Fig. 2E), suggesting that ISARL functions as a metabolic moderator in ticks.

ISARL-mediated phospholipid metabolic pathways affect *B. burgdorferi* colonization

To further investigate the exact metabolism pathway(s) involving in *B. burgdorferi* colonization, we first selected 18 well-annotated and metabolism-related differentially expressed genes to validate the accuracy and reproducibility of the transcriptome bioinformatic analyses by qPCR. The samples for qPCR validation are independent of the sequencing samples. In general, the qPCR results indicated that all the tested genes showed concordant direction of change with the RNA-seq bioinformatic data except one gene, pyridoxine kinase (*PDXK*) (Fig. S3), indicating the accuracy and reliability of our RNA-seq libraries. Of these 17 down-regulated genes, four genes showed significant downregulation profiles ($P < 0.05$). These four genes included phosphatidylserine synthase I (*PTDSS1*) (Figs 2F and 2G), N-CAM Ig domain-containing protein (*NCAM*),

vacuolar H+-ATPase V1 sector, subunit G (*V-ATPase*), and sideroflexin 1,2,3, putative (*SFXN*) (Fig. S4A).

Then, we silenced these four genes individually and investigated their potential roles in *B. burgdorferi* colonization. We also silenced another four genes, whose *P*-values were very close to significant (Fig. S4B). These four genes included 3-hydroxyacyl-CoA dehydrogenase, putative (*3HADH*), adenylosuccinate synthetase (*ADSS*), GMP synthase, putative (*GMPS*), and alpha-actinin, putative (*ACTN*). We did not observe a significant decrease of *B. burgdorferi* burden in nymphal tick guts after silencing *NCAM*, *V-ATPase*, *SFXN*, *ADSS*, *GMPS*, and *ACTN* compared to ds *GFP*-injected ticks (Fig. S5). Instead, we found that *PTDSS1*-silenced nymphs showed a marked reduction in the *B. burgdorferi* burden in the guts when compared to that in control ticks ($P < 0.05$) (Fig. 2H). Furthermore, a blood meal containing *B. burgdorferi* resulted in significantly increased expression of *PTDSS1* in the nymphal tick guts ($P < 0.05$) (Fig. 2I), suggesting that PTDSS1 indeed has a critical role during *B. burgdorferi* colonization of the tick gut. PTDSS1 is involved in phospholipid metabolism, and mainly uses L-serine as the phosphatidyl acceptor to generate the anionic lipid phosphatidylserine (PS), which serves as a precursor for phosphatidylethanolamine (PE) and phosphatidylcholine (PC) synthesis (Fig. 2J) (Aktas et al., 2014). Importantly, PC is one of the main phospholipids on the cellular membrane of *B. burgdorferi* (Kerstholt et al., 2020). However, *B. burgdorferi* lacks the central phospholipid metabolic enzymes. To further validate that the phospholipid metabolic pathway in tick is critical for *B. burgdorferi*, we silenced another enzyme (ISARL-unrelated), phosphatidylserine decarboxylase (*PSD*, ISCI003338), which is an important

239 enzyme in the synthesis of PE in both prokaryotes and eukaryotes (Voelker, 1997).
240 Interestingly, we also found a significantly decreased *B. burgdorferi* burden in ds *PSD*-
241 injected tick guts ($P < 0.05$), and PSD and PTDSS1 elicit a similar degree of reduced *B.*
242 *burgdorferi* levels (Fig. 2K). Taken together, ISARL-mediated phospholipid metabolic
243 pathways associated with PTDSS1 have a critical role in *B. burgdorferi* colonization.
244
245 **Mammalian adiponectin regulates tick glucose metabolism pathway but has no**
246 **effect on *B. burgdorferi* colonization**
247
248 We further explored how the ISARL signaling pathway is activated in ticks.
249 Although the *I. scapularis* genome encodes an adiponectin receptor homolog, an
250 adiponectin ligand is not present, at least in currently annotated *Ixodes* genome
251 databases. This suggests that ticks may utilize vertebrate adiponectin to activate the
252 adiponectin receptor during a blood meal, that tick have another ligand that stimulates the
253 receptor, or both. Since ticks are habitually exposed to adiponectin present during a
254 bloodmeal, we examined whether the tick adiponectin receptor could interact with
255 incoming mammalian adiponectin during blood feeding. We injected recombinant mouse
256 adiponectin into unfed ticks and investigated whether mammalian adiponectin could
257 activate downstream signaling of tick adiponectin receptor by RNA-seq (Fig. 3A). The
258 data showed that one classic downstream gene of mammalian adiponectin signaling, tick
259 glucose-6-phosphatase (*G6P*, ISCW017459), was significantly downregulated in the
260 presence of mammalian adiponectin (Fig. 3A; Table S3). It has been demonstrated that
261 in mammals, the binding of adiponectin to its receptor suppresses *G6P* and

phosphoenolpyruvate carboxykinase (*PEPCK*) expression through an AMP-activated protein kinase (AMPK)-dependent mechanism, which further inhibits glycogenolysis and gluconeogenesis (Fig. 3B) (Tishinsky, 2012). We further searched *G6P* and *PEPCK* homologs in *I. scapularis* genome, and two *G6P* homologs (ISCW017459 and ISCW018612) and three *PEPCK* homologs (ISCW001902, and ISCW000524, ISCW001905) were identified. We designated them as *G6P1*, *G6P2, PEPCK1*, *PEPCK2*, and *PEPCK3*, respectively. We evaluated gene expression of all these five genes after injection of recombinant adiponectin and GFP proteins. Interestingly, *G6P1*, *G6P2, PEPCK2*, and *PEPCK3* were significantly downregulated in the tick gut in the presence of adiponectin (Fig. 3C). To further validate the effects on tick glucose metabolism of interaction of mammalian adiponectin and tick ISARL, we fed ticks on C57BL/6J mice deficient in adiponectin (Adipo$^{-/-}$) and wild-type (WT) animals, and allowed them to feed to repletion (Fig. 3D). We then evaluated the expression of five *G6P* and *PEPCK* genes, and found that *G6P1* and *G6P2* also showed significant downregulation in the presence of adiponectin ($P < 0.05$), while *PEPCK* gene expression was not altered ($P > 0.05$) (Fig. 3E).

To investigate whether the interaction of adiponectin and the receptor in ticks influences *B. burgdorferi* colonization, pathogen-free nymphs were placed on *B. burgdorferi*-infected WT and Adipo$^{-/-}$ mice and allowed to feed to repletion (Fig. 3F). No significant difference of the *B. burgdorferi* burden in ticks feeding on WT and Adipo$^{-/-}$ mice was noted ($P > 0.05$) (Fig. 3G). We also silenced the *G6P1* and *G6P2* genes to determine whether G6P-mediated glucose metabolic changes affect *B. burgdorferi* colonization.

Consistent with the previous observation, there was no significant difference in the *B. burgdorferi* burden between control and *G6P1*-silenced ticks ($P > 0.05$) (Fig. S6A). *G6P2*-silenced ticks also did not show altered *B. burgdorferi* levels ($P > 0.05$) (Fig. S6B). Furthermore, the expression of *G6P1* and *G6P2* in the nymphs was not influenced by *B. burgdorferi* infection ($P > 0.05$) (Fig. S6C), suggesting that G6P1- or G6P2-mediated changes do not affect *B. burgdorferi* colonization of the tick gut. To assess any changes in the adiponectin concentration in murine serum after *B. burgdorferi* infection, the mice were injected subcutaneously with 100 uL containing $1x10^4$ or $1x10^7$ *B. burgdorferi,* or PBS as a control. We found that *B. burgdorferi* does not influence the adiponectin concentration in murine blood (Fig. 3H). Taken together, these data suggest that mammalian adiponectin can regulate ISARL-mediated glucose metabolism pathway, however, it has no effect on *B. burgdorferi* colonization.

B. burgdorferi **interacts with ISARL through tick C1QL3 protein**

We therefore examined whether *I. scapularis* protein(s) might interact with ISARL and if *B. burgdorferi* could influence this process -- for *ISARL* silencing diminished *B. burgdorferi* colonization. To this end, we performed a blastp search of the *I. scapularis* genome with the globular C1Q domain of human and mouse adiponectin, which is known to stimulate the adiponectin receptor (Yamauchi et al., 2002). Two tick proteins had blastp hits with the human adiponectin C1Q domain (Fig. 4A) and were annotated as complement C1q-like protein 3 (C1QL3) (GenBank number: XP_002415101) and conserved hypothetical protein (GenBank number: EEC18766), respectively. These are

identical proteins except that C1QL3 has a signal peptide sequence and we therefore focused on C1QL3.

We first examined whether expression of *C1QL3* could be stimulated by *B. burgdorferi* infection. A blood meal containing *B. burgdorferi* resulted in significantly increased expression of *C1QL3* in the nymphal tick guts ($P < 0.01$) (Fig. 4B). We then generated *C1QL3*-silenced nymphs and found that these ticks had a marked reduction of the *B. burgdorferi* burden in the guts when compared to that in control *I. scapularis* ($P < 0.05$) (Fig. 4C). This is the same observation as with silencing of *ISARL*, suggesting that *B. burgdorferi* activates the ISARL-signaling pathway through the tick C1QL3 protein. Because C1QL3 C1Q domain has high similarity (64.0%) with the human adiponectin C1Q domain (Fig. S7), and C1Q proteins have been demonstrated to activate diverse pathways through the adiponectin receptor (Zheng et al., 2011), we investigated whether tick C1QL3 could interact with ISARL. Human embryonic kidney HEK293T cells were transfected with the ISARL expression vector (pEZT-ISARL). The results showed that tick ISARL can be successfully expressed, as validated by cell staining and western blot (Figs 4D and 4E), on the HEK293T cell membrane (Fig. 4D). We then generated tick C1QL3 protein in a *Drosophila* expression system (Fig. 4F). The HEK293T cells were then incubated with the recombinant C1QL3 protein. After washing and staining, recombinant C1QL3 could be detected on the surface of ISARL-expressed rather than empty plasmid transfected HEK293T cells (Fig. 4G). A pull-down assay also indicated that recombinant C1QL3 interacts with ISARL as demonstrated by the detection of C1QL3 only in ISARL expressed cells pellet (Fig. 4H). In addition, co-immunolocalization demonstrated that the

C1QL3 protein specifically binds to the ISARL-expressed cell membrane (Fig. 4I). These results suggest that tick C1QL3 interacts with ISARL.

Since C1QL3 is a ligand of tick ISARL and also involved in *Borrelia* colonization, we further investigated whether C1QL3 has a role on the activation of ISARL by *Borrelia*. We first assessed if silencing of *C1QL3* influenced *ISARL* expression after feeding on *B. burgdorferi*-infected mice (Fig. 5A). QPCR assessment showed that the *ISARL* transcript level following RNAi silencing of *C1QL3* was significantly lower than that in control ds *GFP*-injected tick guts after feeding on *B. burgdorferi*-infected mice ($P < 0.05$) (Fig. 5B). More importantly, after silencing *C1QL3*, a blood meal containing *B. burgdorferi* did not significantly increase expression of *ISARL* in the nymphal tick guts as compared to feeding on clean mice ($P > 0.05$) (Fig. 5C), further suggesting that C1QL3 plays a role in the ISARL signaling pathways.

Discussion

Adiponectin is a hormone, secreted mainly from adipocytes, that stimulates glucose utilization and fatty acid oxidation (Berg et al., 2001; Fruebis et al., 2001). The key roles of adiponectin in regulating energy homeostasis are mediated by adiponectin receptors across species including humans, yeast, nematodes, and flies (Kwak et al., 2013; Narasimhan et al., 2005; Svensson et al., 2011; Yamauchi et al., 2003). In this study, we have identified and characterized an adiponectin receptor homologue from *I. scapularis*, ISARL. ISARL shares significant sequence similarities with human, mouse, and *Drosophila* adiponectin receptors. In addition, ISARL contains the canonical features of adiponectin receptors, including conserved TM domains, a long internal N-terminal region, and a relatively short external C-terminal region. The highly conserved amino acids and the structures of ISARL and the receptor from *D. melanogaster* suggest that their ligands and signaling pathways may also be conserved in arthropods. However, homologs of adiponectin have not yet been identified in arthropods, suggesting that ligands for adiponectin receptors in arthropods may interact in different ways that in vertebrates.

The Lyme disease agent, *B. burgdorferi*, engages in intimate interactions with *I. scapularis* during its acquisition and colonization of the tick gut (Radolf et al., 2012). This is accompanied by dramatic changes in the expression profiles of *Borrelia* and tick gut genes, which are critical drivers for colonization, persistence or transmission (Kurokawa et al., 2020; Narasimhan et al., 2017). In our study, expression of *ISARL* was significantly

368 increased in the nymphal tick gut after *B. burgdorferi* infection. The upregulation of *ISARL*
369 correlates with *Borrelia* infection in the gut. More interestingly, after silencing *ISARL*
370 expression in the tick gut by anal pore injection, nymphal tick guts showed a marked
371 reduction in the *B. burgdorferi* burden when compared to that in control ticks,
372 demonstrating that ISARL facilitates *B. burgdorferi* colonization.
373
374 We utilized RNA-seq to elucidate the pathways that are altered when *ISARL* is
375 silenced in ticks that engorge on clean and *B. burgdorferi*-infected mice. All the
376 differentially expressed genes were downregulated, and GO functional classification and
377 KEGG pathways also showed that the most downregulated genes are involved in fatty
378 acid, lipid and phospholipid, purine, amino acid, glycerophospholipid, and carbohydrate
379 metabolism and transport pathways. Therefore, ISARL in ticks functions as a metabolic
380 regulator.
381
382 Importantly, ISARL can regulate a critical enzyme involved in phospholipid
383 metabolism, PTDSS1. Regulation of PTDSS1 by adiponectin receptors is also found in
384 other organisms such as yeast, where the adiponectin receptor homolog Izh2 is
385 connected to phospholipid metabolism through co-regulation of the expression of inositol-
386 3-phosphate synthase (*INO1*) and phosphatidylserine synthase (*CHO1*, homolog of
387 *PTDSS1*) genes with zinc-responsive activator protein (*Zap1*) (Ušaj et al., 2015).
388 Silencing of *I. scapularis PTDSS1* led to a reduced spirochete burden in the guts, thereby
389 linking *B. burgdorferi* colonization with phospholipid metabolism. The *B. burgdorferi*
390 genome is small and encodes a limited number of metabolic enzymes (Casjens et al.,

2000; Fraser et al., 1997). The restricted biosynthetic capability forces *B. burgdorferi* to rely on its vertebrate and arthropod hosts for nutrients or enzymes that it cannot synthesize (Tilly et al., 2008). Interestingly, we also found that silencing of *I. scapularis 3HADH,* which is involved in fatty acid metabolic processes, decreased the *B. burgdorferi* burden in tick gut (Figure S5D). The markedly decreased *B. burgdorferi* burden in ticks after silencing of *PTDSS1*, *PSD* and *3HADH*, suggests that the spirochete may require the tick for selected metabolic needs.

We also found that *B. burgdorferi* can interact with an adiponectin-related protein, C1QL3, in ticks, which associates with ISARL. The interactions lead to phospholipid metabolism changes in ticks. We propose that C1QL3 in tick is mainly involved in metabolism, rather than complement activation, as demonstrated by the decreased *B. burgdorferi* level after silencing C1QL3. Indeed, some of C1Q/TNF family proteins are associated with metabolism. In addition to adiponectin, proteins such as C1Q/TNF-related protein 3 (CTRP3), CTRP5, CTRP9, CTRP13 (C1QL3), and CTRP15 also belong to adipokine family, and have been reported to be associated with the regulation of glucose, lipid or other metabolisms (Jiang et al., 2018; Li et al., 2011; Mi et al., 2019; Wei et al., 2011; Wolf et al., 2016). Importantly, C1Q proteins have been demonstrated to activate diverse pathways through adiponectin receptor (Zheng et al., 2011).

In summary, we demonstrate that ISARL plays a key role in metabolic pathways in *I. scapularis*. ISARL-mediated phospholipid metabolism by PTDSS1 contributes to *B. burgdorferi* colonization and an adiponectin-related protein, C1QL3, is involved in ISARL

414 signaling pathway. These studies elucidate a new pathway involved in tick metabolism,
415 and demonstrate that *B. burgdorferi* co-opts the activation of this pathway to facilitate
416 colonization of *I. scapularis*. These processes are crucial to understanding the complex
417 life cycle of the Lyme disease agent within ticks, and may be applicable to other
418 arthropods and arthropod-borne infectious agents.
419

Materials and Methods

Ethics statement

Animal care and housing were performed according to the Guide for the Care and Use of laboratory Animals of National Institutes of Health, USA. All protocols in this study were approved by the Yale University Institutional Animal Care and Use Committee (YUIACUC) (approval number 2018-07941). All animal experiments were performed in a Biosafety Level 2 animal facility.

Mice, spirochetes, ticks, and cells

C3H/HeJ mice, C57BL/6J mice wild-type (WT), and C57BL/6J mice deficient in adiponectin (Adipo$^{-/-}$) were purchased from the Jackson Laboratory (https://www.jax.org/strain/008195). All mice were bred and maintained in a pathogen-free facility at Yale University. The spirochetes *B. burgdorferi* N40 were grown at 33℃ in Barbour-Stoenner-Kelly H (BSK-H) complete medium (Sigma-Aldrich, #B8291) with 6% rabbit serum. The live cell density was ~10^6-10^7 cells/mL as determined by dark field microscopy and hemocytometric analysis. To obtain *B. burgdorferi*-infected mice, the mice were injected subcutaneously with 100 uL of *B. burgdorferi* N40 (1x10^5 cells/mL). Two weeks after inoculation, the *B. burgdorferi* burden in mice was assayed by qPCR analysis of spirochete DNA in murine ear punch biopsies as described below. DNA was extracted from mouse skin-punch biopsies using the DNeasy tissue kit (QIAGEN, #69506)

443 according to the manufacturer's protocol. The DNA was analyzed by qPCR using
444 *flagellinB* (*flaB*) primers, and data was normalized to mouse *actin*. The primer sequences
445 are shown in Table S4. Pathogen-free *I. scapularis* larvae were acquired from the Centers
446 for Disease Control and Prevention. The larval ticks were fed to repletion on pathogen-
447 free C3H/HeJ mice and allowed to molt to nymphs. *B. burgdorferi*-infected nymphs were
448 generated by placing larvae on *B. burgdorferi*-infected C3H/HeJ mice, and fed larvae
449 were molted to nymphs. Nymphal ticks were maintained at 85% relative humidity with a
450 14h light and 10h dark period at 23 °C. Human embryonic kidney HEK293T cells (ATCC,
451 #CRL-3216) was used for vitro studies. The HEK293T cells were grown in Dulbecco's
452 Modified Eagle's Medium (DMEM, ThermoFisher, #11965-118) media supplemented with
453 10% Fetal Bovine Serum (FBS, Sigma, #12306C-500).
454
455 **Identification and characterization of the *I. scapularis* adiponectin receptor-like**
456 **(*ISARL*) gene**
457
458 The human adiponectin receptor protein 1 (GenBank number: NP_001277482)
459 and 2 (GenBank number: NP_001362293) sequences were used to conduct tblastn and
460 blastp searches against the available black-legged tick database (taxid:6945) using NCBI
461 default parameters. Tick adiponectin receptor sequence was further validated by
462 amplification with primers in Table S4. Multiple alignment of protein sequences were
463 performed using the Clustal Omega (https://www.ebi.ac.uk/Tools/msa/clustalo/) (Madeira
464 et al., 2019) or Uniprot (https://www.uniprot.org/align/). The similarities of adiponectin
465 receptor protein sequences were measured in EMBOSS supermatcher

(https://www.bioinformatics.nl/cgi-bin/emboss/supermatcher). The protein structure of ISARL was predicted in SWISS-MODEL (https://swissmodel.expasy.org/) (Guex and Peitsch, 1997; Waterhouse et al., 2018). Hydrophobicity analysis was performed using ProtScale (https://web.expasy.org/protscale/) (Gasteiger et al., 2005).

Tick exposure to *B. burgdorferi* and expression of *ISARL*

To evaluate gene expression of *ISARL* upon *B. burgdorferi* infection, pathogen-free *I. scapularis* nymphs were placed on *B. burgdorferi*-free and -infected mice (C3H/HeJ). At least three mice were used in each experiment, and the ticks were allowed to feed to repletion. Both *B. burgdorferi*-free and -exposed tick guts were dissected under the dissecting microscope. The RNA from dissected guts was purified by Trizol (Invitrogen, #15596-018) following the manufacturer's protocol, and cDNA was synthesized using the iScript cDNA Synthesis Kits (Bio-Rad, #1708891). qPCR was performed using iQ SYBR Green Supermix (Bio-Rad, #1725124) on a Bio-Rad cycler with a program consisting of an initial denaturing step of 2 min at 95°C and 45 amplification cycles consisting of 20 s at 95°C followed by 15 s at 60°C, and 30 s at 72°C. The genes and corresponding primer sequences are shown in Table S4. The specific target transcripts of *ISARL* and the reference gene tick *actin* were quantified by extrapolation from a standard curve derived from a series of known DNA dilutions of each target gene, and data was normalized to tick *actin*.

RNAi silencing of targeted genes

Fed-nymph gut cDNA was prepared as described above and used as template to amplify segments of targeted genes. The PCR primers with T7 promoter sequences are shown in Table S4. Double-stranded RNA (dsRNA) were synthesized using the MEGAscript RNAi kit (Invitrogen, #AM1626M) using PCR-generated DNA template that contained the T7 promoter sequence at both ends. The dsRNA quality was examined by agarose gel electrophoresis. DsRNA of the *Aequorea victoria* green fluorescent protein (GFP) was used as a control. Pathogen-free and -infected tick nymphs were injected in the anal pore with dsRNA (6 nL) using glass capillary needles as described by Narasimhan and colleagues (2004).

Effects of silenced genes on *B. burgdorferi* colonization and transmission

To examine the effects of silencing targeted genes on the colonization of *B. burgdorferi* in the tick gut, dsRNA microinjected pathogen-free *I. scapularis* nymphs were placed on *B. burgdorferi*-infected mice (C3H/HeJ) and allowed to feed to repletion. The ticks were then collected for gut dissection. The *B. burgdorferi* burden in the tick gut was quantified by amplifying *flaB*. *FlaB* was quantified by extrapolation from a standard curve derived from a series of known DNA dilutions of *flaB* gene, and data was normalized to tick *actin*. The knockdown efficiency of targeted genes was tested as described above. Specifically, the expression of targeted genes was estimated with the $\Delta\Delta C_T$ method (Schmittgen and Livak, 2008) using the reference gene *actin*. To test the effects of silencing *ISARL* on the transmission of *B. burgdorferi*, a group of three to five *GFP* or

512 *ISARL* dsRNA injected *B. burgdorferi*-infected nymphs were placed on each C3H/HeJ
513 mouse (at least five mice each in the *GFP* or *ISARL* dsRNA groups) and allowed to feed
514 to repletion. Ticks are placed on the mouse head/back between the ears. At 7 and 14
515 days-post tick detachment, the mice were anesthetized, and skin was aseptically punch
516 biopsied and assessed for spirochete burden by qPCR. Ticks feed in head area and skin
517 punch biopsies are collected from the pinnae /ears. This site is considered distal as it is
518 not at the site of tick bite. Twenty-one days post tick detachment, the mice were sacrificed,
519 and ear skin, heart, and joints were aseptically collected and assessed for spirochete
520 burden by qPCR.
521
522 **RNA-seq and bioinformatic analyses**
523
524 DsRNA (ds *ISARL* and ds *GFP*) microinjected pathogen-free *I. scapularis* nymphs
525 were placed on clean and *B. burgdorferi*-infected mice (C3H/HeJ), respectively, and
526 allowed to feed to repletion. Then, the ticks were collected for gut dissection. Total RNA
527 was purified as described above. In addition, to check the transcriptional alterations in the
528 tick gut in the presence of mammalian adiponectin, pathogen-free tick nymphs were
529 injected in the anal pore with recombinant mouse adiponectin (MilliporeSigma, #SRP3297)
530 and GFP proteins (SinoBiological, #13105-S07E). Then, the guts were dissected after 8h
531 injection, and RNA was purified. The RNA samples were then submitted for library
532 preparation using TruSeq (Illumina, San Diego, CA, USA) and sequenced using Illumina
533 HiSeq 2500 by paired-end sequencing at the Yale Centre for Genome Analysis (YCGA).
534 The *I. scapularis* transcript data was downloaded from the VectorBase

(https://vectorbase.org/vectorbase/app/) (Giraldo-Calderon et al., 2015) and indexed using the kallisto-index (Bray et al., 2016). The reads from the sequencer were pseudo-aligned with the index reference transcriptome using kallisto (Bray et al., 2016). The counts generated were processed by DESeq2 (Love et al., 2014) in RStudio (https://rstudio.com). Gene ontology (GO) enrichment analysis and Kyoto Encyclopedia of Genes and Genomes (KEGG) pathway enrichment analyses were conducted using the functional annotation tool DAVID 6.8 (Sherman and Lempicki, 2009).

Recombinant mouse adiponectin (Sigma, #SRP3297) and GFP protein (Sino Biological, #13105-S07E) were injected into pathogen-free *I. scapularis* nymphs. After 8h, the ticks were collected for gut dissection. Total RNA was purified and RNA-seq and analyses were performed as described above.

Expression of ISARL and binding assays

Tick *ISARL* gene was PCR amplified from nymph cDNA using the primer pair listed in Table S4, then cloned into the *Xba*I and *Not*I sites of the pEZT-Dlux, a modified pEZT-BM vector (Addgene, #74099) in-frame with a HA-tag sequence, by Gibson Assembly Cloning Kit (NEB, #E5510S). HEK293T cells were transfected with the *ISARL* expression plasmid (pEZT-ISARL) using TransIT 2020 (Mirus, #MIR5404). After 40 h post transfection, the cells were washed with 1X PBS and then incubated with rC1QL3 protein with His/V5 tag, respectively. After 16 h incubation with gentle agitation, the cells were washed with PBS and fixed in 4% PFA for 15 min at room temperature. Then, the cells

were blocked in 1% BSA in PBS for 1 h, and subsequently immunolabeled with anti-HA antibody (1:100, Cell Signaling Technology, #C29F4) for checking ISARL expression, and V5 tag monoclonal antibody (1:100, Invitrogen, # R960-25) for checking C1QL3 binding. Cells were washed with PBS three times and then immunolabeled with secondary antibodies of Goat anti-Rabbit IgG (H+L) Highly Cross-Adsorbed Secondary Antibody, Alexa Fluor 488 (1:100, Invitrogen, #A-11034) and Goat anti-Mouse IgG (H+L) Cross-Adsorbed Secondary Antibody, Alexa Fluor 555 (1:100, Invitrogen, #A-21422) for 1 h at room temperature. Nuclei were stained with DAPI (Invitrogen, #D9542). After staining, the fluorescence signals were examined with an EVOS FL Auto Cell Imaging System (Thermo Fisher Scientific). We also conducted plot profile to help analyze co-localization by Image J software.

For checking ISARL expression by western blot, after 40 h post transfection, the cells were washed with 1X PBS and then lysed with 4X Laemmli Sample Buffer (Bio-Rad, #1610747). After centrifuge at high speed, the supernatant was loaded to perform western blot as described below. HRP Anti-His tag antibody (1:10,000, abcam, #ab3553) or anti-HA antibody (1:1000, Cell Signaling Technology, #C29F4) was used to detect expression of ISARL.

We conducted a pull-down assay to check the binding of ISARL and C1QL3 as described in Schuijt et al. (2011a). Briefly, HEK293T cells were transfected as described above. After 40 h post transfection, the cells were washed and suspended with 1X PBS and then incubated with rC1QL3 protein for 16 h with gentle agitation, respectively. Then

the cells were pelleted, and the pellet and supernatant were separated. The pellet was washed five to eight times in 1.5 ml PBS/0.1% BSA and was resuspended in the same volume as the supernatant. Equal volumes of supernatant and pellet were used to run western blot as described below. HRP V5-tag monoclonal antibody (1:1000, Invitrogen, # R961-25) was used to detect protein.

Adiponectin concentration in serum after *B. burgdorferi* infection

To assess the adiponectin concentration change in mice serum after *B. burgdorferi* infection, the C3H/HeJ mice were injected subcutaneously with 100 uL $1x10^4$ and $1x10^7$ cells/mL *B. burgdorferi* and PBS as a control (five mice in each group). At 0, 21 and 28 days-post inoculation, the blood was collected from mice. The sera were separated from mice blood samples by centrifugation at 1000 x g for 10 min at 4 °C. The adiponectin in mice serum was quantified by Mouse Adiponectin/Acrp30 Quantikine ELISA Kit (R&D Systems, #MRP300).

Effects of adiponectin in mice blood on *B. burgdorferi* colonization

Pathogen-free *I. scapularis* nymphs were placed on *B. burgdorferi*-infected WT and Adipo$^{-/-}$ mice (C57BL/6J) and allowed to feed to repletion. The ticks were then collected for gut dissection. The *B. burgdorferi* burden in the tick gut was quantified as described above.

Purification of recombinant proteins

The *C1QL3* was PCR amplified from tick nymph cDNA using the primer pair listed in Table S4, then cloned into the *Bgl*II and *Xho*I sites of the pMT/BiP/V5-His vector (Invitrogen, #V413020). The recombinant protein was expressed and purified using the *Drosophila* Expression System as described previously (Schuijt et al., 2011b). The protein was purified from the supernatant by TALON metal affinity resin (Clontech, #635606) and eluted with 150 mM imidazole. The eluted samples were filtered through a 0.22-μm filter and concentrated with a 10-kDa concentrator (MilliporeSigma, #Z740203) by centrifugation at 4 °C. Recombinant protein purities were assessed by SDS-PAGE using 4-20% Mini-Protean TGX gels (Bio-Rad, #4561094) and quantified using the BCA Protein Estimation kit (ThermoFisher Scientific, #23225).

Western blot

Proteins were separated by SDS-PAGE at 160 V for 1h. Proteins were transferred onto a 0.45-m-pore-size polyvinylidene difluoride (PVDF) membrane (Bio-Rad, #1620177) and processed for immunoblotting. The blots were blocked in 1% non-fat milk in PBS for 60 min. Primary antibodies of PTDSS1 Rabbit pAb (1:1000, Abclonal, #A13065), Anti-beta Actin antibody (1:1000, abcam, #ab8224), HRP Anti-6X His tag antibody (1:10,000, abcam, #ab3553) or HRP V5 tag monoclonal antibody (1:1000, Invitrogen, # R961-25) were diluted in 0.05% PBST and incubated with the blots for 1 h at room temperature or 4 °C overnight. HRP-conjugated secondary antibody (1:2500, Invitrogen, #62-6520 and

627 #31466) were diluted in PBST and incubated for 1 h at room temperature. After washing
628 with PBST, the immunoblots were imaged and quantified with a LI-COR Odyssey imaging
629 system.
630
631 **Statistical analysis**
632
633 Statistical significance of differences observed in experimental and control groups
634 was analyzed using GraphPad Prism version 8.0 (GraphPad Software, Inc., San Diego,
635 CA). Non-parametric Mann-Whitney test or unpaired t test were utilized to compare the
636 mean values of control and tested groups, and $P < 0.05$ was considered significant. The
637 exact *P* values are shown in the source data.

References

Aktas, M., L. Danne, P. Möller, and F. Narberhaus. 2014. Membrane lipids in Agrobacterium tumefaciens: biosynthetic pathways and importance for pathogenesis. *Frontiers in plant science* 5:109.

Asch, E., D. Bujak, M. Weiss, M. Peterson, and A. Weinstein. 1994. Lyme disease: an infectious and postinfectious syndrome. *The Journal of rheumatology* 21:454-461.

Berg, A.H., T.P. Combs, X. Du, M. Brownlee, and P.E. Scherer. 2001. The adipocyte-secreted protein Acrp30 enhances hepatic insulin action. *Nature medicine* 7:947-953.

Bray, N.L., H. Pimentel, P. Melsted, and L. Pachter. 2016. Near-optimal probabilistic RNA-seq quantification. *Nat Biotechnol* 34:525-527.

Buechler, C., J. Wanninger, and M. Neumeier. 2010. Adiponectin receptor binding proteins–recent advances in elucidating adiponectin signalling pathways. *FEBS letters* 584:4280-4286.

Casjens, S., N. Palmer, R. Van Vugt, W. Mun Huang, B. Stevenson, P. Rosa, R. Lathigra, G. Sutton, J. Peterson, and R.J. Dodson. 2000. A bacterial genome in flux: the twelve linear and nine circular extrachromosomal DNAs in an infectious isolate of the Lyme disease spirochete Borrelia burgdorferi. *Molecular microbiology* 35:490-516.

Estrada-Peña, A., and F. Jongejan. 1999. Ticks feeding on humans: a review of records on human-biting Ixodoidea with special reference to pathogen transmission. *Experimental & applied acarology* 23:685-715.

Fraser, C.M., S. Casjens, W.M. Huang, G.G. Sutton, R. Clayton, R. Lathigra, O. White, K.A. Ketchum, R. Dodson, and E.K. Hickey. 1997. Genomic sequence of a Lyme disease spirochaete, Borrelia burgdorferi. *Nature* 390:580-586.

Fruebis, J., T.-S. Tsao, S. Javorschi, D. Ebbets-Reed, M.R.S. Erickson, F.T. Yen, B.E. Bihain, and H.F. Lodish. 2001. Proteolytic cleavage product of 30-kDa adipocyte complement-related protein increases fatty acid oxidation in muscle and causes weight loss in mice. *Proceedings of the National Academy of Sciences* 98:2005-2010.

Gasteiger, E., C. Hoogland, A. Gattiker, M.R. Wilkins, R.D. Appel, and A. Bairoch. 2005. Protein identification and analysis tools on the ExPASy server. In The proteomics protocols handbook. Springer, 571-607.

Giraldo-Calderon, G.I., S.J. Emrich, R.M. MacCallum, G. Maslen, E. Dialynas, P. Topalis, N. Ho, S. Gesing, C. VectorBase, G. Madey, F.H. Collins, and D. Lawson. 2015. VectorBase: an updated bioinformatics resource for invertebrate vectors and other organisms related with human diseases. *Nucleic Acids Res* 43:D707-713.

Guex, N., and M.C. Peitsch. 1997. SWISS-MODEL and the Swiss-Pdb Viewer: an environment for comparative protein modeling. *electrophoresis* 18:2714-2723.

Jiang, F., M. Yang, X. Zhao, R. Liu, G. Yang, D. Liu, H. Liu, H. Zheng, Z. Zhu, and L. Li. 2018. C1q/TNF-Related Protein5 (CTRP5) as a biomarker to predict metabolic

682 syndrome and each of its components. *International journal of endocrinology*
683 2018:
684 Kadowaki, T., T. Yamauchi, N. Kubota, K. Hara, K. Ueki, and K. Tobe. 2006.
685 Adiponectin and adiponectin receptors in insulin resistance, diabetes, and the
686 metabolic syndrome. *The Journal of clinical investigation* 116:1784-1792.
687 Karpichev, I.V., L. Cornivelli, and G.M. Small. 2002. Multiple regulatory roles of a novel
688 Saccharomyces cerevisiae protein, encoded by YOL002c, in lipid and phosphate
689 metabolism. *Journal of Biological Chemistry* 277:19609-19617.
690 Kerstholt, M., M.G. Netea, and L.A. Joosten. 2020. Borrelia burgdorferi hijacks cellular
691 metabolism of immune cells: Consequences for host defense. *Ticks and Tick-*
692 *borne Diseases* 11:101386.
693 Kurokawa, C., G.E. Lynn, J.H. Pedra, U. Pal, S. Narasimhan, and E. Fikrig. 2020.
694 Interactions between Borrelia burgdorferi and ticks. *Nature Reviews Microbiology*
695 1-14.
696 Kwak, S.-J., S.-H. Hong, R. Bajracharya, S.-Y. Yang, K.-S. Lee, and K. Yu. 2013.
697 Drosophila adiponectin receptor in insulin producing cells regulates glucose and
698 lipid metabolism by controlling insulin secretion. *PLoS One* 8:e68641.
699 Li, Y., G.L. Wright, and J.M. Peterson. 2011. C1q/TNF-related protein 3 (CTRP3)
700 function and regulation. *Comprehensive Physiology* 7:863-878.
701 Love, M.I., W. Huber, and S. Anders. 2014. Moderated estimation of fold change and
702 dispersion for RNA-seq data with DESeq2. *Genome Biol* 15:550.
703 Madeira, F., Y.M. Park, J. Lee, N. Buso, T. Gur, N. Madhusoodanan, P. Basutkar, A.R.
704 Tivey, S.C. Potter, and R.D. Finn. 2019. The EMBL-EBI search and sequence
705 analysis tools APIs in 2019. *Nucleic acids research* 47:W636-W641.
706 Mi, Q., Y. Li, M. Wang, G. Yang, X. Zhao, H. Liu, H. Zheng, and L. Li. 2019. Circulating
707 C1q/TNF-related protein isoform 15 is a marker for the presence of metabolic
708 syndrome. *Diabetes/metabolism research and reviews* 35:e3085.
709 Narasimhan, M.L., M.a.A. Coca, J. Jin, T. Yamauchi, Y. Ito, T. Kadowaki, K.K. Kim, J.M.
710 Pardo, B. Damsz, and P.M. Hasegawa. 2005. Osmotin is a homolog of
711 mammalian adiponectin and controls apoptosis in yeast through a homolog of
712 mammalian adiponectin receptor. *Molecular cell* 17:171-180.
713 Narasimhan, S., R.R. Montgomery, K. DePonte, C. Tschudi, N. Marcantonio, J.F.
714 Anderson, J.R. Sauer, M. Cappello, F.S. Kantor, and E. Fikrig. 2004. Disruption
715 of Ixodes scapularis anticoagulation by using RNA interference. *Proceedings of*
716 *the National Academy of Sciences* 101:1141-1146.
717 Narasimhan, S., T.J. Schuijt, N.M. Abraham, N. Rajeevan, J. Coumou, M. Graham, A.
718 Robson, M.-J. Wu, S. Daffre, and J.W. Hovius. 2017. Modulation of the tick gut
719 milieu by a secreted tick protein favors Borrelia burgdorferi colonization. *Nature*
720 *communications* 8:1-17.
721 Ouchi, N., and K. Walsh. 2007. Adiponectin as an anti-inflammatory factor. *Clinica*
722 *chimica acta* 380:24-30.
723 Radolf, J.D., M.J. Caimano, B. Stevenson, and L.T. Hu. 2012. Of ticks, mice and men:
724 understanding the dual-host lifestyle of Lyme disease spirochaetes. *Nature*
725 *reviews microbiology* 10:87-99.
726 Rosenberg, R., N.P. Lindsey, M. Fischer, C.J. Gregory, A.F. Hinckley, P.S. Mead, G.
727 Paz-Bailey, S.H. Waterman, N.A. Drexler, and G.J. Kersh. 2018. Vital signs:

trends in reported vectorborne disease cases—United States and Territories, 2004–2016. *Morbidity and Mortality Weekly Report* 67:496.

Schmittgen, T.D., and K.J. Livak. 2008. Analyzing real-time PCR data by the comparative C T method. *Nature protocols* 3:1101.

Schuijt, T.J., J. Coumou, S. Narasimhan, J. Dai, K. DePonte, D. Wouters, M. Brouwer, A. Oei, J.J. Roelofs, and A.P. van Dam. 2011a. A tick mannose-binding lectin inhibitor interferes with the vertebrate complement cascade to enhance transmission of the lyme disease agent. *Cell host & microbe* 10:136-146.

Schuijt, T.J., S. Narasimhan, S. Daffre, K. DePonte, J.W. Hovius, C. Van't Veer, T. van der Poll, K. Bakhtiari, J.C. Meijers, and E.T. Boder. 2011b. Identification and characterization of Ixodes scapularis antigens that elicit tick immunity using yeast surface display. *PLoS One* 6:e15926.

Sherman, B.T., and R.A. Lempicki. 2009. Systematic and integrative analysis of large gene lists using DAVID bioinformatics resources. *Nature protocols* 4:44.

Singh, S., and H. Girschick. 2004. Lyme borreliosis: from infection to autoimmunity. *Clinical Microbiology and Infection* 10:598-614.

Steere, A.C., V.K. Sikand, F. Meurice, D.L. Parenti, E. Fikrig, R.T. Schoen, J. Nowakowski, C.H. Schmid, S. Laukamp, and C. Buscarino. 1998. Vaccination against Lyme disease with recombinant Borrelia burgdorferi outer-surface lipoprotein A with adjuvant. *New England Journal of Medicine* 339:209-215.

Svensson, E., L. Olsen, C. Mörck, C. Brackmann, A. Enejder, N.J. Faergeman, and M. Pilon. 2011. The adiponectin receptor homologs in C. elegans promote energy utilization and homeostasis. *PLoS One* 6:e21343.

Tilly, K., P.A. Rosa, and P.E. Stewart. 2008. Biology of infection with Borrelia burgdorferi. *Infectious disease clinics of North America* 22:217-234.

Tishinsky, J. 2012. Modulation of adipokines by n-3 polyunsaturated fatty acids and ensuing changes in skeletal muscle metabolic response and inflammation. In.

Ušaj, M.M., M. Prelec, M. Brložnik, C. Primo, T. Curk, J. Ščančar, L. Yenush, and U. Petrovič. 2015. Yeast Saccharomyces cerevisiae adiponectin receptor homolog Izh2 is involved in the regulation of zinc, phospholipid and pH homeostasis. *Metallomics* 7:1338-1351.

Voelker, D.R. 1997. Phosphatidylserine decarboxylase. *Biochimica et Biophysica Acta (BBA)-Lipids and Lipid Metabolism* 1348:236-244.

Waterhouse, A., M. Bertoni, S. Bienert, G. Studer, G. Tauriello, R. Gumienny, F.T. Heer, T.A.P. de Beer, C. Rempfer, and L. Bordoli. 2018. SWISS-MODEL: homology modelling of protein structures and complexes. *Nucleic acids research* 46:W296-W303.

Wei, Z., J.M. Peterson, and G.W. Wong. 2011. Metabolic regulation by C1q/TNF-related protein-13 (CTRP13): activation OF AMP-activated protein kinase and suppression of fatty acid-induced JNK signaling. *Journal of Biological Chemistry* 286:15652-15665.

Wolf, R.M., K.E. Steele, L.A. Peterson, X. Zeng, A.E. Jaffe, M.A. Schweitzer, T.H. Magnuson, and G.W. Wong. 2016. C1q/TNF-related protein-9 (CTRP9) levels are associated with obesity and decrease following weight loss surgery. *The Journal of Clinical Endocrinology & Metabolism* 101:2211-2217.

773 Yamauchi, T., J. Kamon, Y. Ito, A. Tsuchida, T. Yokomizo, S. Kita, T. Sugiyama, M.
774 Miyagishi, K. Hara, and M. Tsunoda. 2003. Cloning of adiponectin receptors that
775 mediate antidiabetic metabolic effects. *Nature* 423:762-769.
776 Yamauchi, T., J. Kamon, Y.a. Minokoshi, Y. Ito, H. Waki, S. Uchida, S. Yamashita, M.
777 Noda, S. Kita, and K. Ueki. 2002. Adiponectin stimulates glucose utilization and
778 fatty-acid oxidation by activating AMP-activated protein kinase. *Nature medicine*
779 8:1288-1295.
780 Yamauchi, T., Y. Nio, T. Maki, M. Kobayashi, T. Takazawa, M. Iwabu, M. Okada-Iwabu,
781 S. Kawamoto, N. Kubota, and T. Kubota. 2007. Targeted disruption of AdipoR1
782 and AdipoR2 causes abrogation of adiponectin binding and metabolic actions.
783 *Nature medicine* 13:332-339.
784 Zheng, Q., Y. Yuan, W. Yi, W.B. Lau, Y. Wang, X. Wang, Y. Sun, B.L. Lopez, T.A.
785 Christopher, and J.M. Peterson. 2011. C1q/TNF-related proteins, a family of
786 novel adipokines, induce vascular relaxation through the adiponectin receptor-
787 1/AMPK/eNOS/nitric oxide signaling pathway. *Arteriosclerosis, thrombosis, and*
788 *vascular biology* 31:2616-2623.
789 Zhu, M., K. Chen, Y. Wang, Z. Guo, H. Yin, Q. Yao, and H. Chen. 2008. Cloning and
790 partial characterization of a gene in Bombyx mori homologous to a human
791 adiponectin receptor. *ACTA Biochimica Polonica* 55:241-249.
792
793
794

ACKNOWLEDGEMENTS

This work was support by grants from the NIH (AI126033, AI138949) and the Steven and Alexandra Cohen Foundation. We sincerely thank Ms Kathleen DePonte for her excellent technical assistance. We would like to acknowledge that figures were created using BioRender.

AUTHOR CONTRIBUTIONS

X.T. and E.F. conceived and shaped the overall direction of the project. X.T. Y.C. G.A. J.H. A.S. A.M. Y.M.C. M.J.W. C.L.B. and H.M. performed experiments. Y.C. and J.H. bred the adiponectin knockout mice. S.M. conducted RNA-seq data analyses. S.N. and U.P. was involved in the critical discussion of this study. Illustrations were created by X.T. using BioRender. X.T. and E.F. wrote the manuscript with feedback and discussions from all co-authors.

DECLARATION OF INTEREST

The authors declare no competing interests.

LEAD CONTACT

Further information and requests for resources and reagents should be directed to and will be fulfilled by the Lead Contact, Erol Fikrig (Erol.Fikrig@yale.edu)

DATA AVAILABILITY

817 The RNA-seq data are available in the Gene Expression Omnibus (GEO) repository at
818 the National Center for Biotechnology Information under the accession number:
819 GSE169293.

Figure legends

Figure 1. Silencing of *ISARL* significantly reduces the *B. burgdorferi* burden in nymphal tick guts. (A) *ISARL* is significantly induced in nymphal tick guts after feeding on *B. burgdorferi*-infected mice. (B) qPCR assessment of *ISARL* transcript levels following RNAi silencing of *ISARL* after feeding on *B. burgdorferi*-infected mice. (C) Nymphal engorgement weights in *ISARL*-silenced and mock-injected nymphs. Each data point represents one engorged tick. (D) qPCR assessment of *B. burgdorferi flaB* levels in guts following RNAi silencing of *ISARL* after feeding on *B. burgdorferi*-infected mice. Each data point represents one nymph gut. Horizontal bars in the above figures represent the median. Statistical significance was assessed using a non-parametric Mann-Whitney test (ns, $P > 0.05$; **, $P < 0.01$; ***, $P < 0.001$; ****, $P < 0.0001$). (E) *Borrelia*-infected nymphs microinjected with ds *ISARL* or ds *GFP* were fed on clean mice to assess transmission of the spirochete. The infection of *Borrelia* in Murine skin 7,14, and 21 days after infection, and in heart and joint tissues at 21 days was determined. (F) Murine skin 7,14, and 21 days after infection, and in heart and joint tissues at 21 days was determined by qPCR of *flaB* and normalized to mouse *actin*. Data represent the means ± standard deviations from five replicates.

Figure 2. **RNA-seq, qPCR validation, and RNAi-silencing assays revealed that phosphatidylserine synthase 1 (*PTDSS1*) is regulated by ISARL and is involved in *B. burgdorferi* colonization.** (A) Hierarchical clustering of differentially expressed genes was generated after feeding on clean mice. (B) Hierarchical clustering of differentially expressed genes was generated after feeding on *B. burgdorferi*-infected mice. The

844 expression levels were visualized and the scale from least abundant to highest range is
845 from -2.0 to 2.0. The phylogenetic relationships of differentially expressed genes are
846 shown on the left tree. The top tree indicated the cluster relationship of the sequenced
847 samples. (C) qPCR validation of *ISARL* knockdown in tick gut. Statistical significance was
848 assessed using a Student's *t* test (*, $P < 0.05$; ****, $P < 0.0001$). (D) Venn diagram
849 depicting unique and common differentially expressed genes between clean and *B.*
850 *burgdorferi*-infected mice feeding. The up arrow indicated upregulation and the down
851 arrow indicated downregulation of differentially expressed genes. (E) Metabolism
852 pathways inferred by GO and KEGG enrichment analyses of transcriptomes comparison
853 between ds *GFP* and ds *ISARL* injection after feeding on *B. burgdorferi*-infected mice to
854 repletion. (F) QPCR validation of *PTDSS1* showed that *PTDSS1* is positively regulated
855 by ISARL. (G) Western blot of PTDSS1 protein showed that PTDSS1 is positively
856 regulated by ISARL (**, $P < 0.05$). (H) qPCR assessment of *PTDSS1* transcript level,
857 nymphal engorgement weights, and *B. burgdorferi flaB* levels in guts following RNAi
858 silencing of *PTDSS1* after feeding on *B. burgdorferi*-infected mice. Each data point
859 represents one nymph. (I) *PTDSS1* is significantly induced in the nymphal tick gut after
860 feeding on *B. burgdorferi*-infected mice. (J) PTDSS1 in involved in phospholipid pathway.
861 Cytidine diphosphate diacylglycerol (CDP-DAG) is converted to phosphatidylserine (PS)
862 by PTDSS1. PE: Phosphatidylethanolamine; PC: Phosphatidylcholine. (K) qPCR
863 assessment of phosphatidylserine decarboxylase (*PSD*) transcript level, nymphal
864 engorgement weights, and qPCR assessment of *B. burgdorferi flaB* levels in guts
865 following RNAi silencing of *PSD* after feeding on *B. burgdorferi*-infected mice. Each data
866 point represents one nymph. Horizontal bars in the above figures represent the median.

867 Statistical significance was assessed using a non-parametric Mann-Whitney test (ns, $P >$
868 0.05; *, $P < 0.05$; **, $P < 0.01$). Source data 1. Source data for PTDSS1 protein relative
869 quantification. Source data 2. Source data for PTDSS1 protein relative quantification.

870
871 **Figure 3**. **Mammalian adiponectin regulates tick glucose metabolism.** (A) RNA-seq
872 of injection of recombinant mouse adiponectin and GFP (control) proteins. One classic
873 downstream gene of mammalian adiponectin receptor signaling, glucose-6-phosphatase
874 (*G6P*), was significantly downregulated in the presence of mammalian adiponectin. (B)
875 Interaction of mammal adiponectin and adiponectin receptor suppresses *G6P* and
876 phosphoenolpyruvate carboxykinase (*PEPCK*) expression through an AMP-activated
877 protein kinase (AMPK)-dependent mechanism, which further inhibits glycogenolysis and
878 gluconeogenesis. (C) Injection of recombinant mouse adiponectin significantly
879 downregulate the expression of *G6P1*, *G6P2, PEPCK2*, and *PEPCK3* in the tick gut. (D)
880 Feed ticks on C57BL/6J WT and Adipo$^{-/-}$ mice and then evaluate the expression of *G6P1*,
881 *G6P2, PEPCK1*, *PEPCK2*, and *PEPCK3*. (E) After feeding on WT and Adipo$^{-/-}$ mice,
882 *G6P1* and *G6P2* showed significant downregulation profile in the presence of adiponectin,
883 while *PEPCK* genes did not exhibit marked downregulation. (F) Ticks were fed on *B.*
884 *burgdorferi*-infected WT and Adipo$^{-/-}$ mice, and then *B. burgdorferi flaB* levels in guts were
885 assessed. (G) qPCR assessment of *B. burgdorferi* burden after feeding on *B. burgdorferi*-
886 infected WT and Adipo$^{-/-}$ mice. No significant difference of *B. burgdorferi* burden in tick
887 gut was observed between feeding on WT and Adipo$^{-/-}$ mice. (H) Adiponectin
888 concentration in mice sera following 21 and 28 days after injection of *B. burgdorferi* at the
889 density of 10^4 and 10^7 cells/mL, respectively. Statistical significance was assessed using
890 a non-parametric Mann-Whitney test (ns, $P > 0.05$; *, $P < 0.05$; **, $P < 0.01$; ***, $P < 0.001$).

Figure 4. **Tick complement C1q-like protein 3 (C1QL3) is involved in ISARL signaling pathways.** (A) Blastp of the tick genome with the human adiponectin C1Q domain in NCBI generated two homologs and were annotated as complement C1q-like protein 3 (C1QL3) (GenBank number: XP_002415101) and conserved hypothetical protein (GenBank number: EEC18766), respectively. These are identical proteins except that C1QL3 has a signal peptide sequence. (B) *C1QL3* is significantly induced in replete nymphal tick guts after feeding on *B. burgdorferi*-infected mice. (C) qPCR assessment of *C1QL3* transcript levels, nymphal engorgement weights, and *B. burgdorferi flaB* levels in guts following RNAi silencing of *C1QL3* after feeding on *B. burgdorferi*-infected mice. (D) Human HEK293T cells were transfected with HA-tagged ISARL-expressing vector (pEZT-ISARL-HA). Forty hours post transfection, the cells were examined. The results showed that ISARL can be successfully expressed on the HEK293T cell membrane. The white arrow indicates examples of membrane expression. (E) Western blot confirmed ISARL expression in the HEK293T cells. (F) Generation of tick C1QL3 protein with His/V5-tag in a *Drosophila* expression system. Recombinant protein was assessed by SDS-PAGE gel and western blot. (G) C1QL3 is bound on the membrane of ISARL-expressed HEK293T cells. 10 X and 20 X are the microscope magnifications. The white arrow indicates one example of binding. (H) Binding of C1QL3 to ISARL as analyzed by a pull-down assay. HRP V5-tag monoclonal antibody was used to detect protein. C1QL3 was only detected in ISARL expressed cells pellet. (I) Co-immunolocalization of ISARL (green) and C1QL3 (red). The specific signal of C1QL3 protein was observed on the surface of some of ISARL expressed cells, and no signal was shown on non-successfully

914 expressed cells membrane. The white arrows indicate examples of binding. Bar: 20 μm.
915 The plot profile of co-localization was conducted by Image J software. Source data 1.
916 Source data for ISARL expression. Source data 2. Source data for C1QL3 protein
917 purification. Source data 3. Source data for C1QL3 protein purification. Source data 4.
918 Source data for binding of C1QL3 to ISARL.
919
920 **Figure 5**. **C1QL3 plays a role on the activation of ISARL by *Borrelia*.** (A) Analysis of
921 how silencing of *C1QL3* influences *ISARL* expression after feeding on *B. burgdorferi*-
922 infected mice. (B) qPCR assessment showed that *ISARL* transcript levels following RNAi
923 silencing of *C1QL3* were significantly lower than that in control ds *GFP*-injected tick guts
924 after feeding on *B. burgdorferi*-infected mice. (C) qPCR assessment showed that a blood
925 meal containing *B. burgdorferi* did not significantly increase expression of *ISARL* in the
926 nymphal tick guts as compared to feeding on clean mice after RNAi silencing of *C1QL3*.
927 Each data point represents one nymph. Horizontal bars in the above figures represent
928 the median. Statistical significance was assessed using a non-parametric Mann-Whitney
929 test (ns, $P > 0.05$; *, $P < 0.05$).
930

931 Figure 1

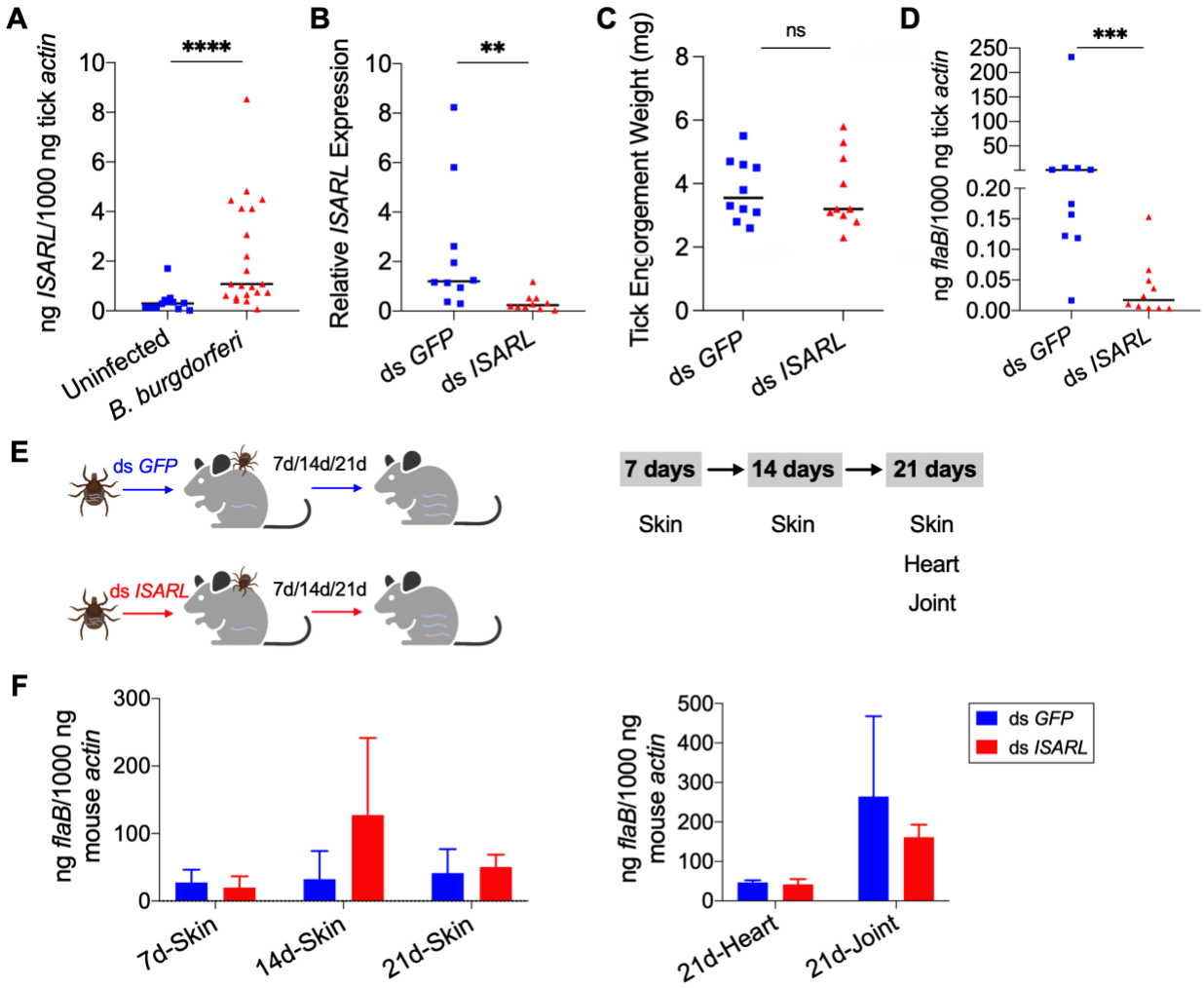

932

933

934

935 Figure 2

936

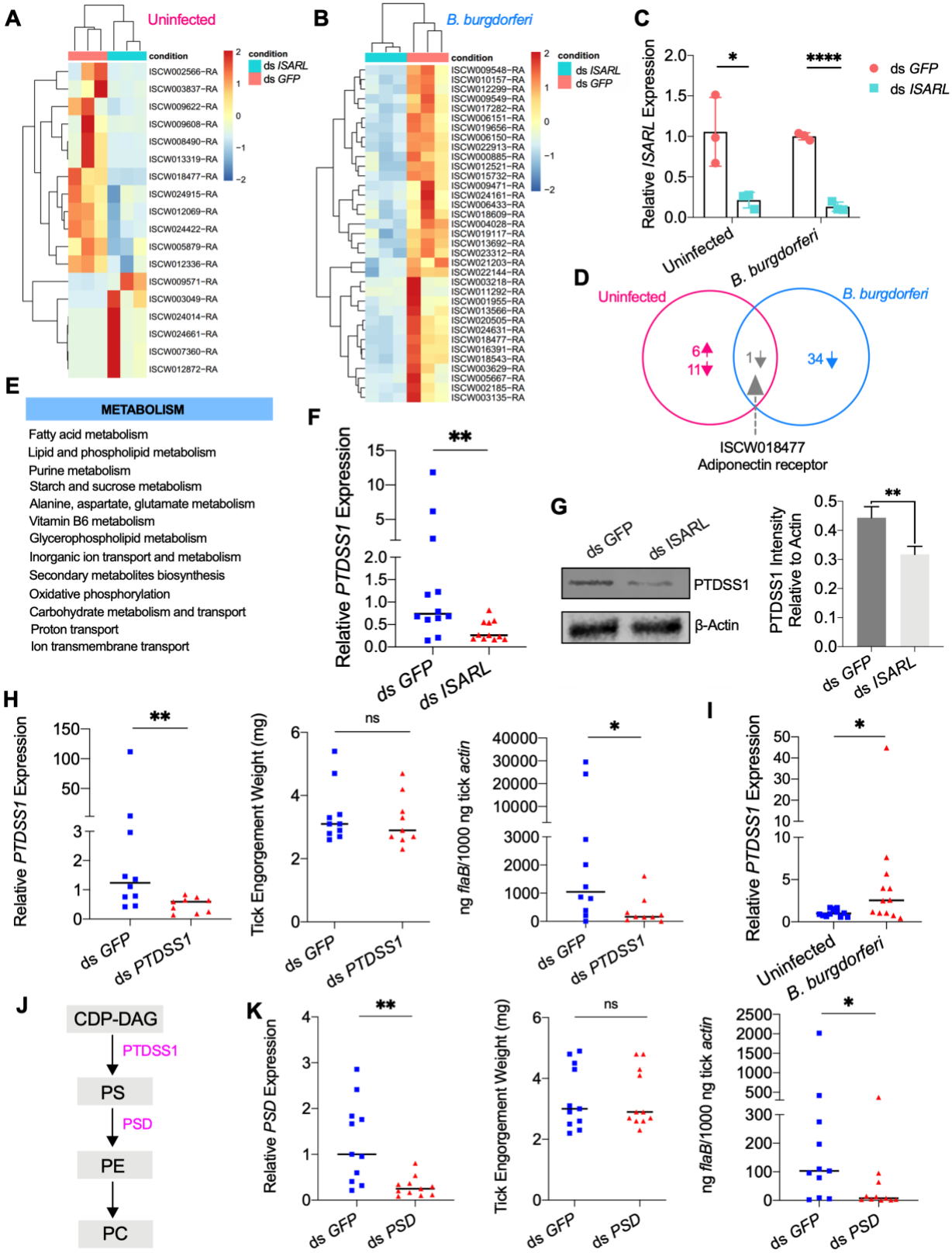

937

938 Figure 3
939

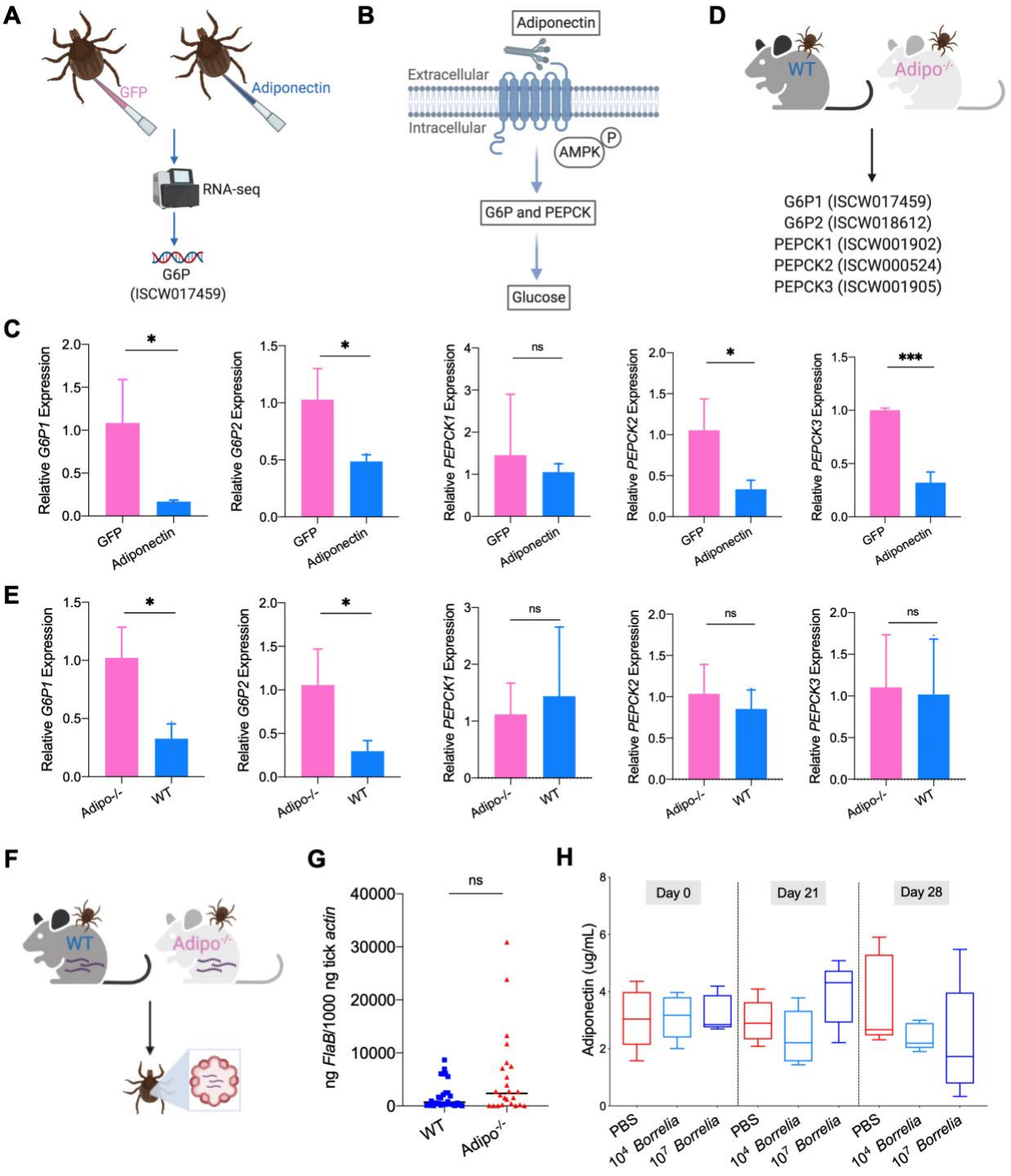

940
941
942
943
944
945

946 Figure 4
947

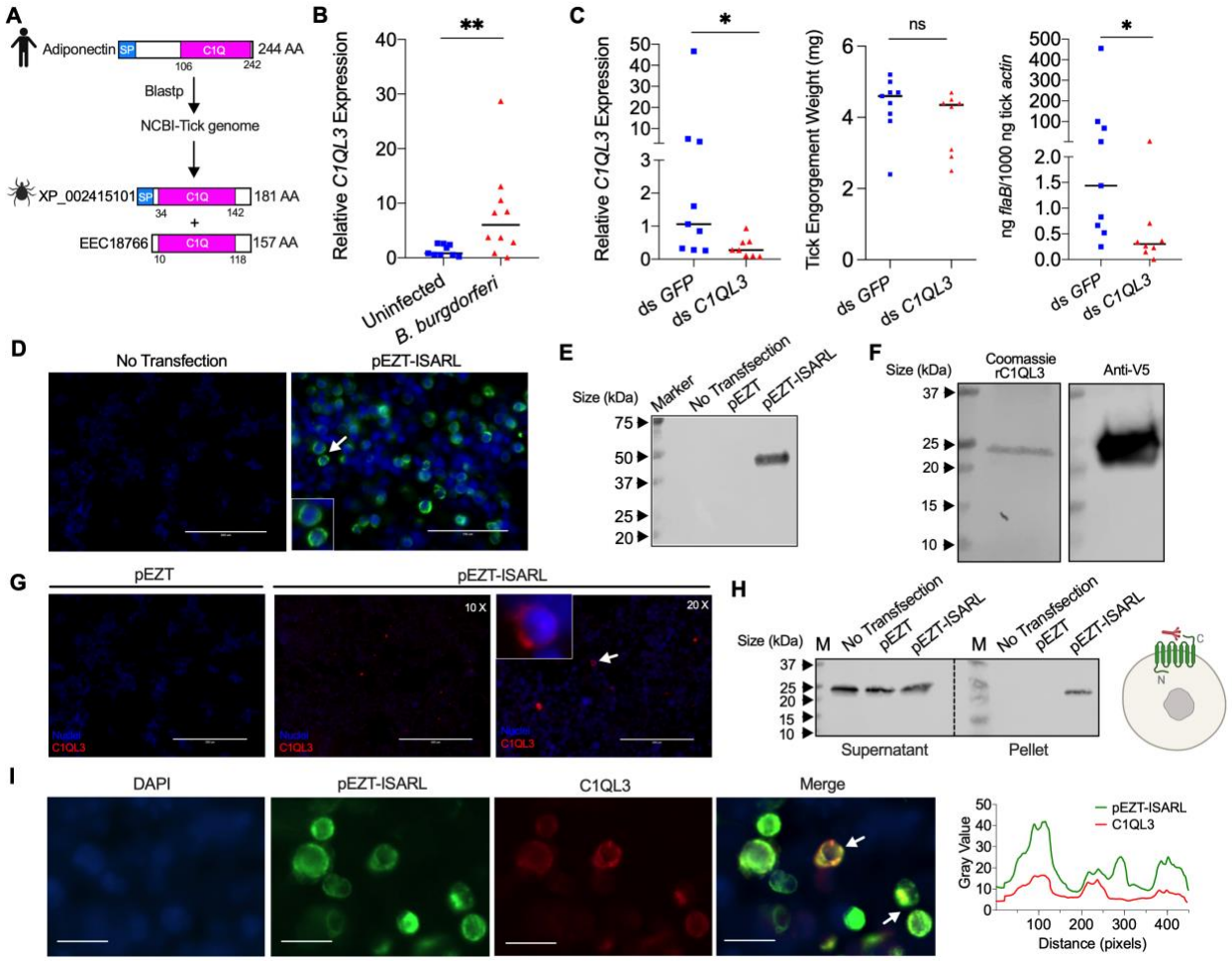

948
949
950

951 Figure 5

952

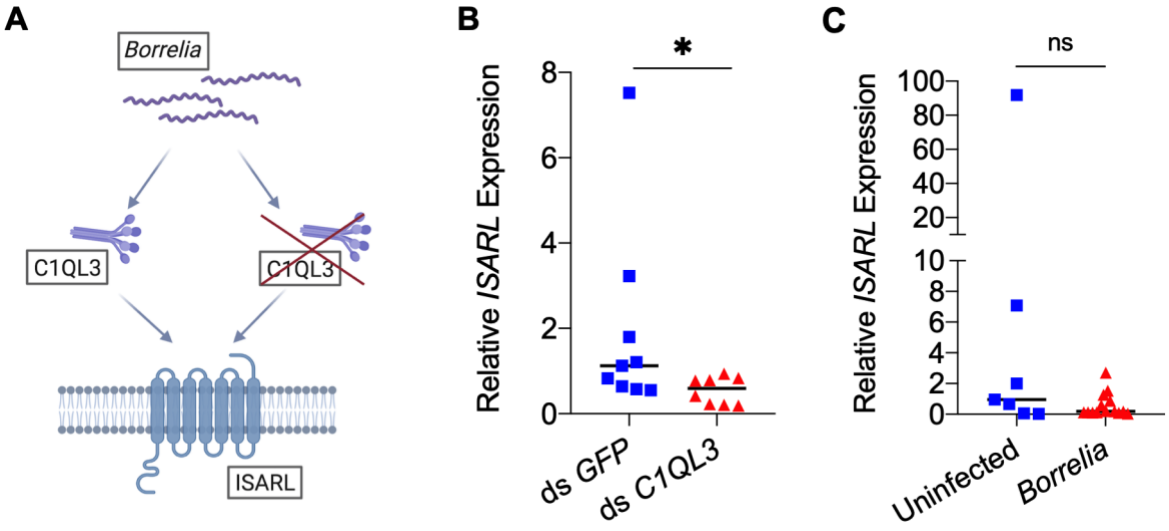

953

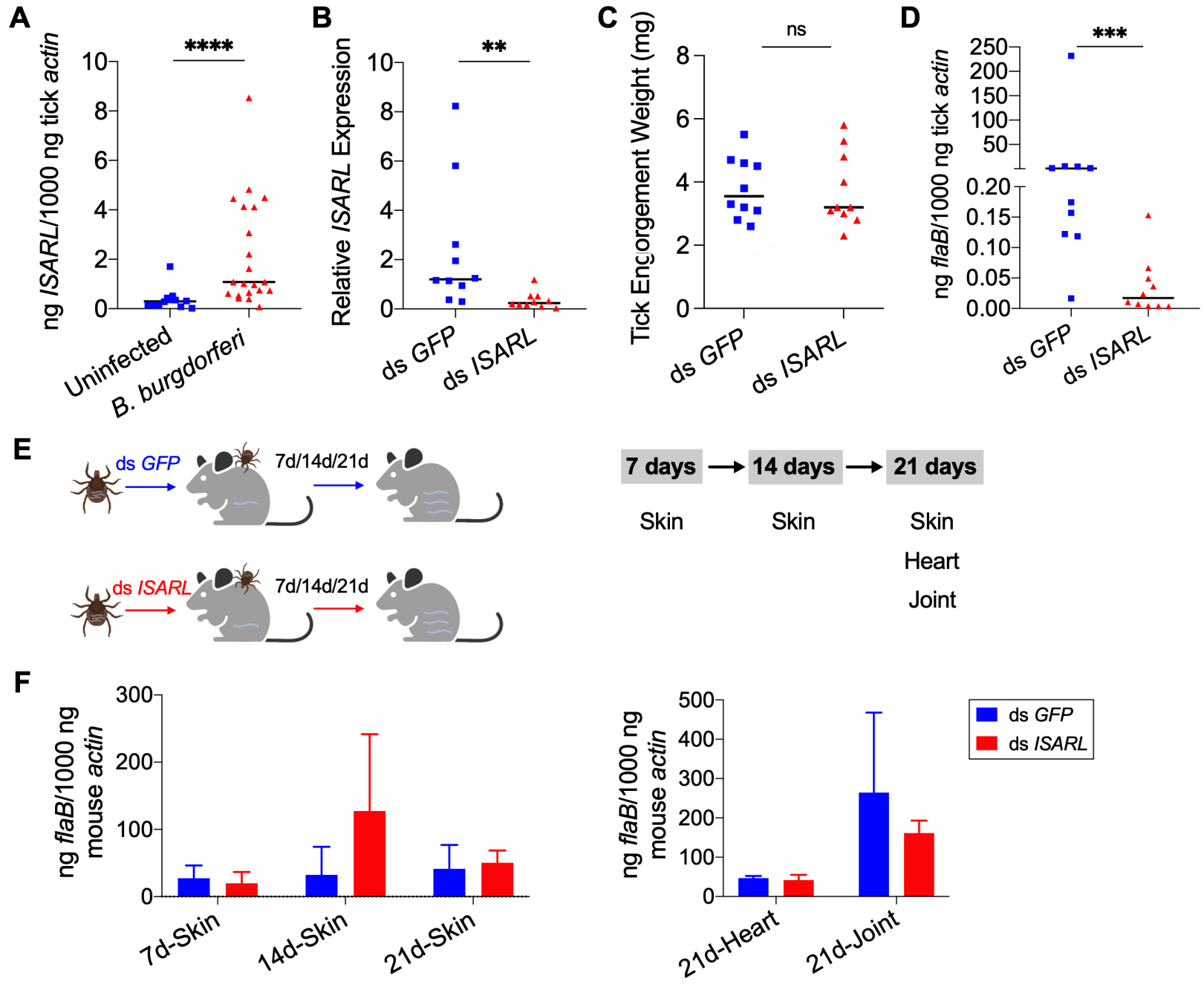

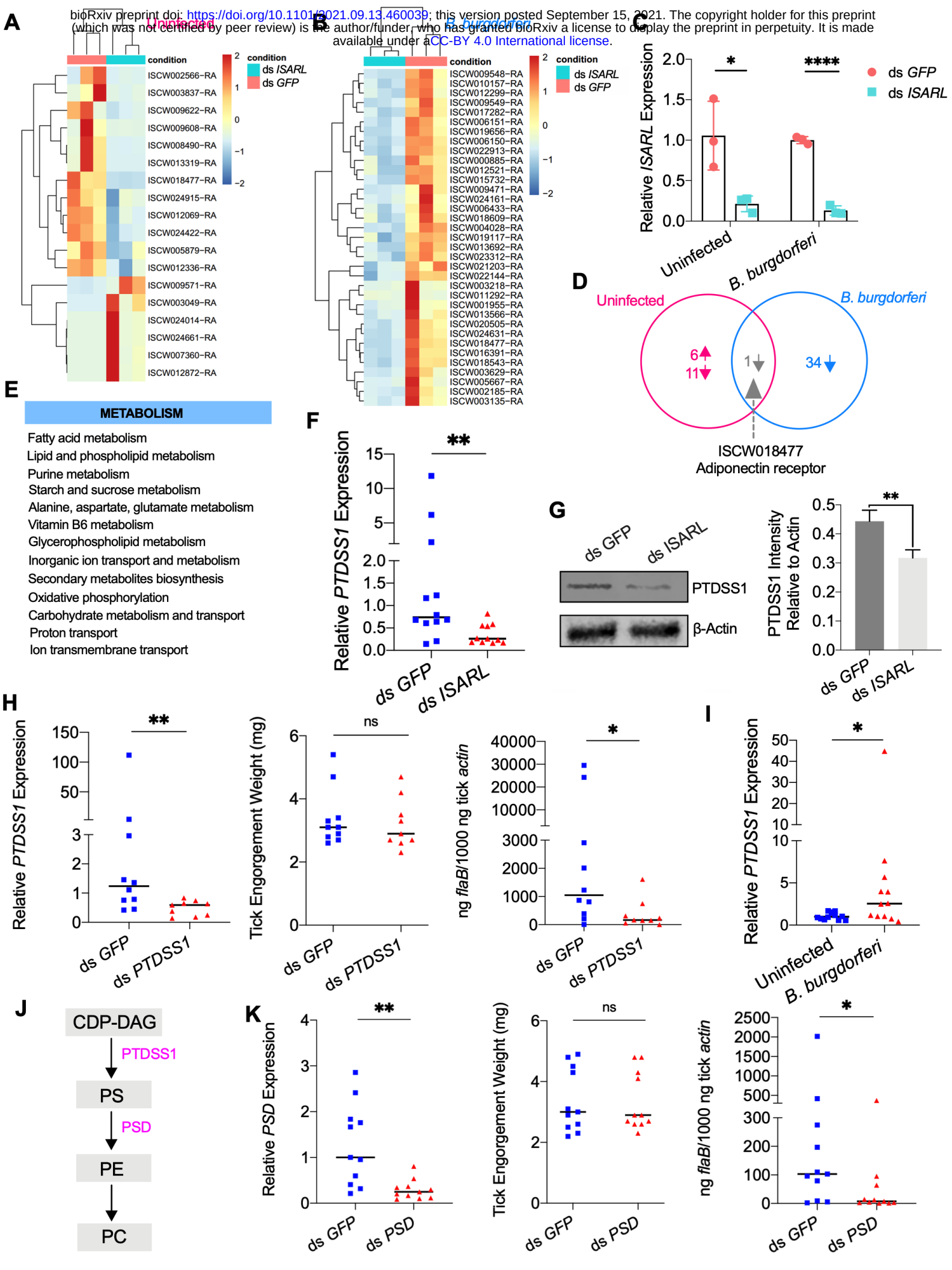

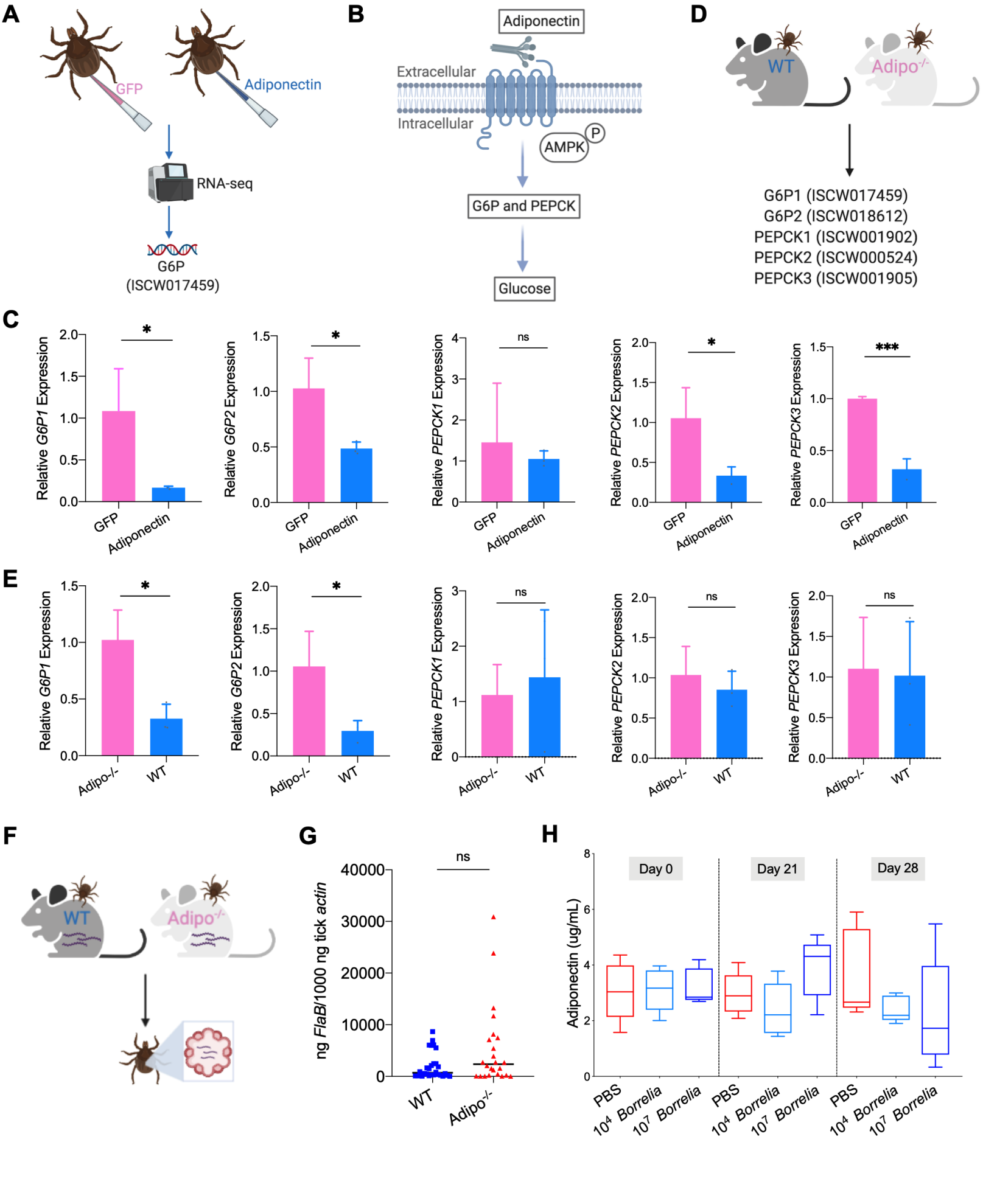

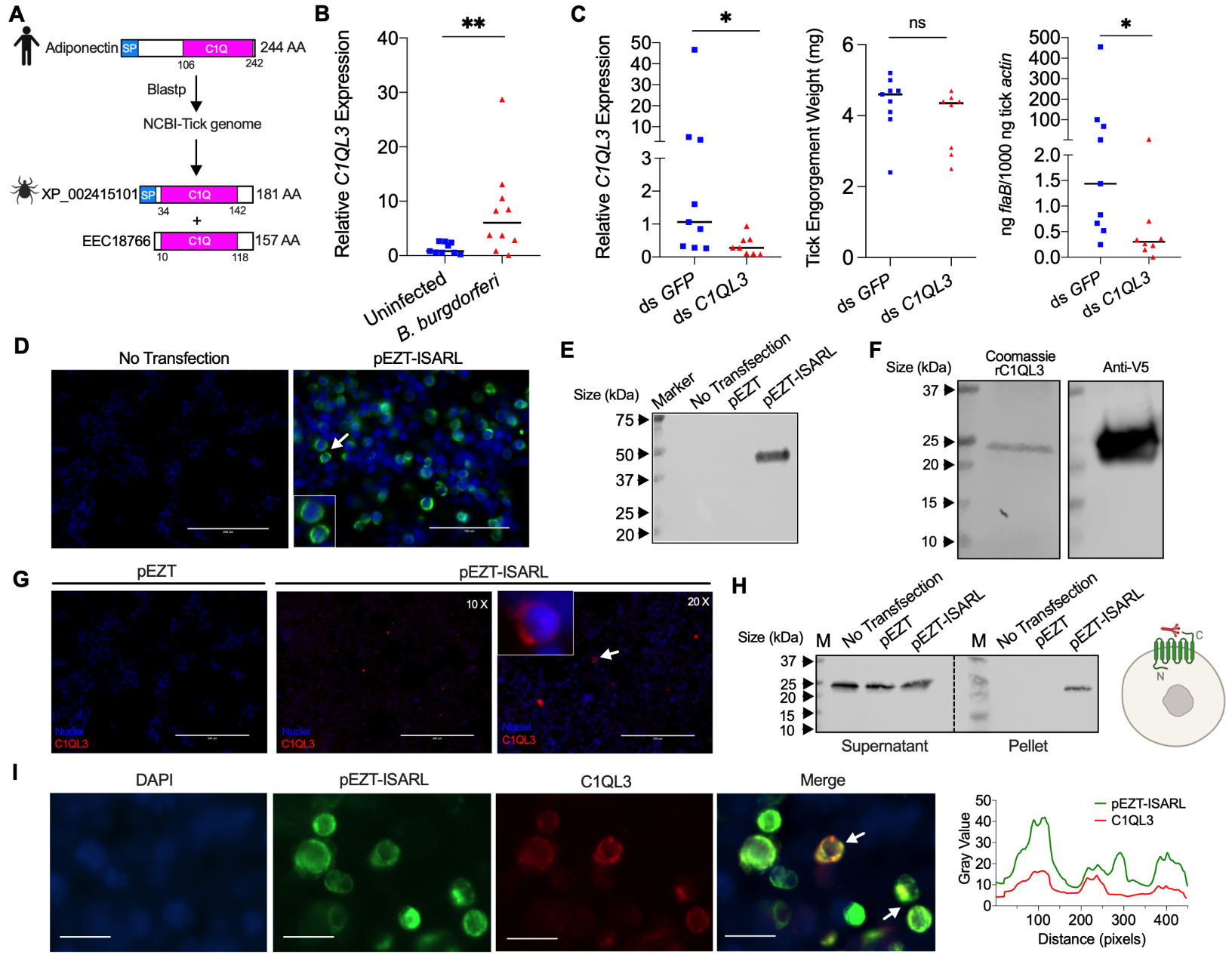

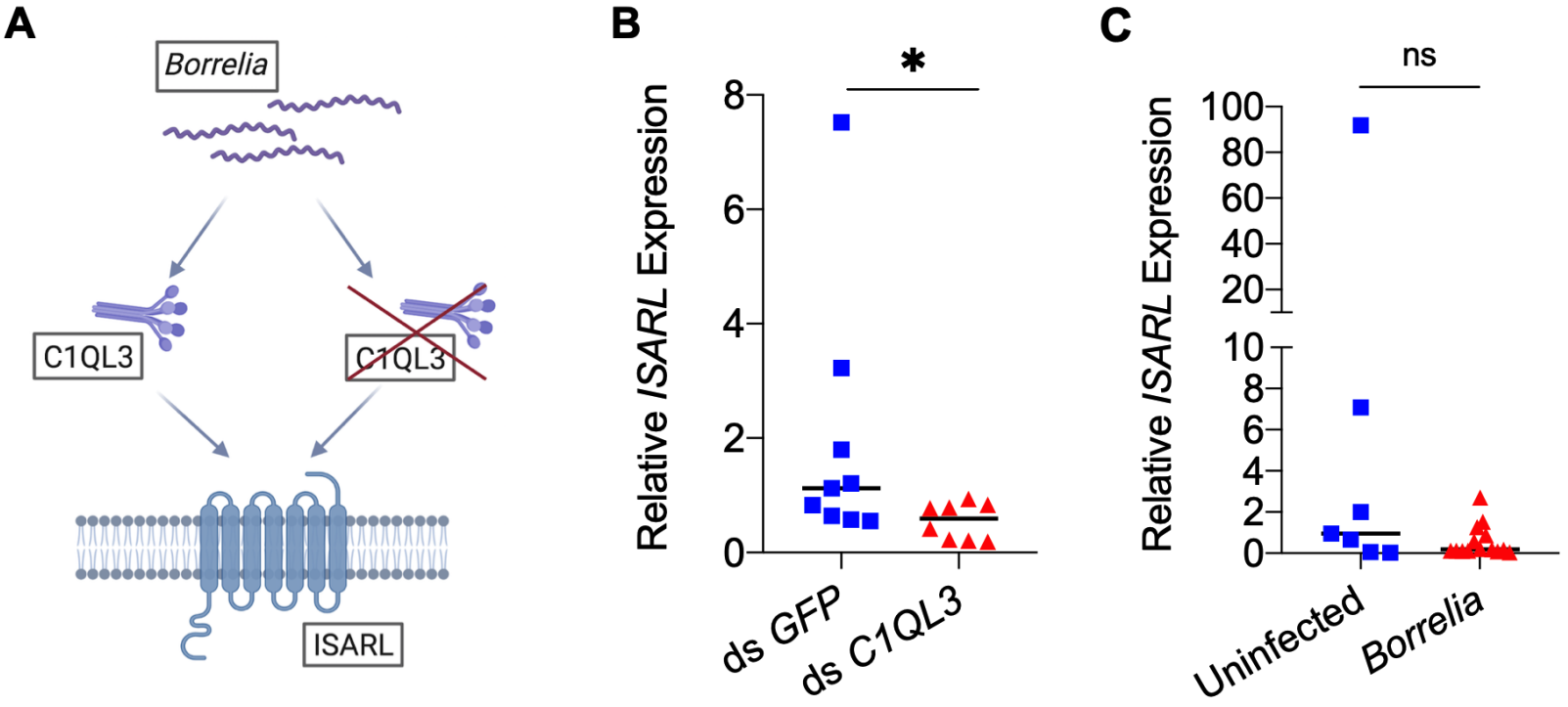

Supplemental information

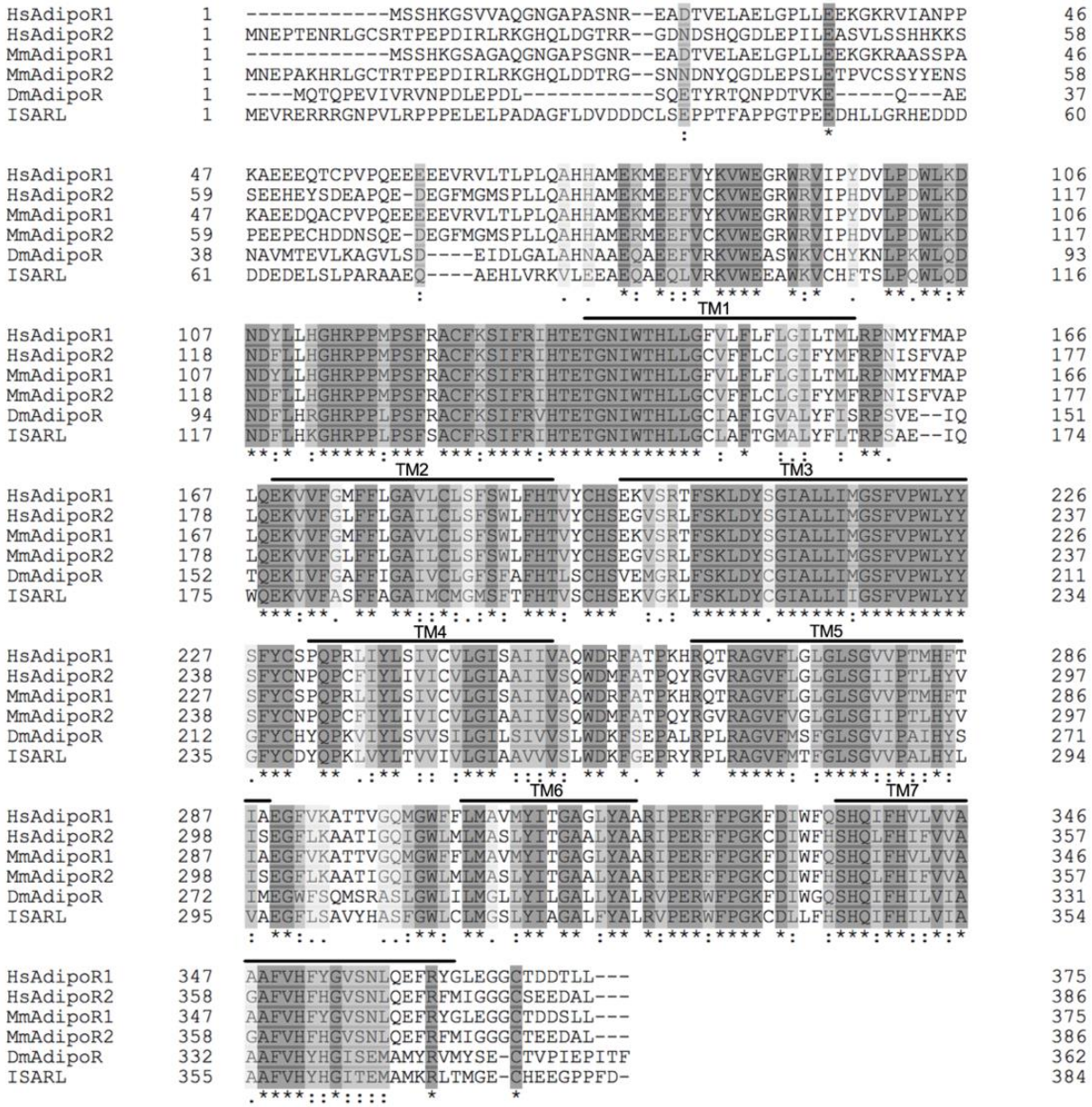

Figure S1. Protein sequence comparison of adiponectin receptors. Multiple sequence alignment of *Ixodes scapularis* ISARL with the amino acid sequences of homologs identified in *Homo sapiens* (NP_001277482, HsAdipoR1; NP_001362293, HsAdipoR2), *Mus musculus* (NP_001292998, MmAdipoR1; NP_001342621, MmAdipoR2), and *Drosophila melanogaster* (NP_732759, DmAdipoR). Seven transmembrane (TM1-TM7) domain regions are marked by upper lines. * indicates

positions which have a single, fully conserved residue (dark grey). : indicates conservation between groups of strongly similar properties (light grey). . indicates conservation between groups of weakly similar properties (white grey). The TM domains is based on the experimentally defined human adiponectin receptors.

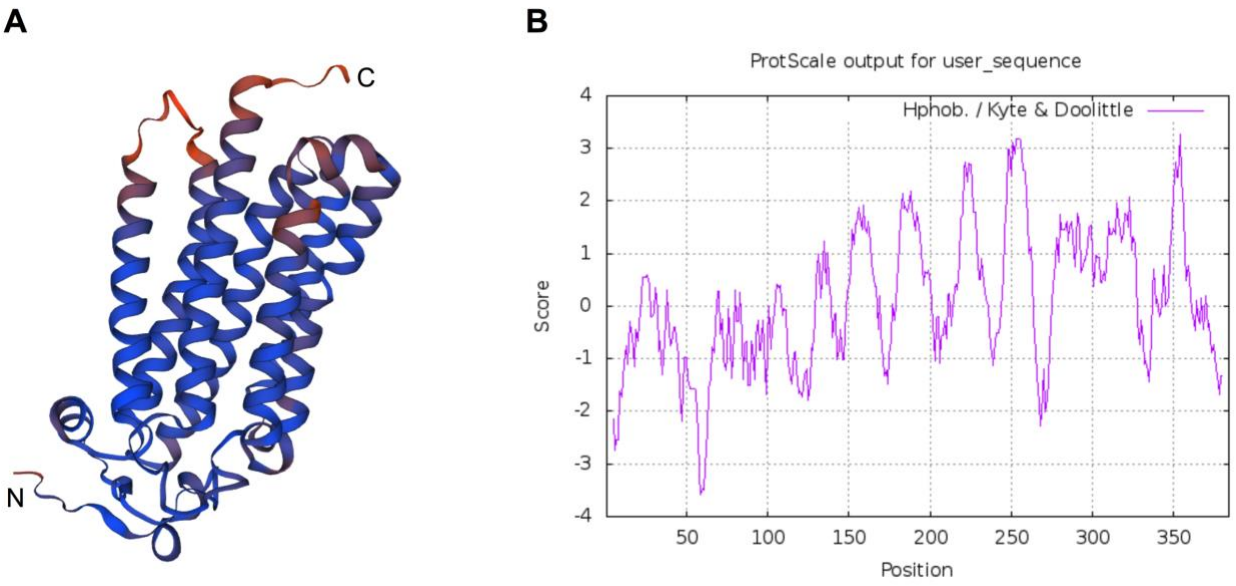

Figure S2. Predicted protein structure and hydrophobicity of ISARL. Seven transmembrane (TM) domains were identified in the ISARL protein based on (A) protein structure prediction and (B) hydrophobicity analysis.

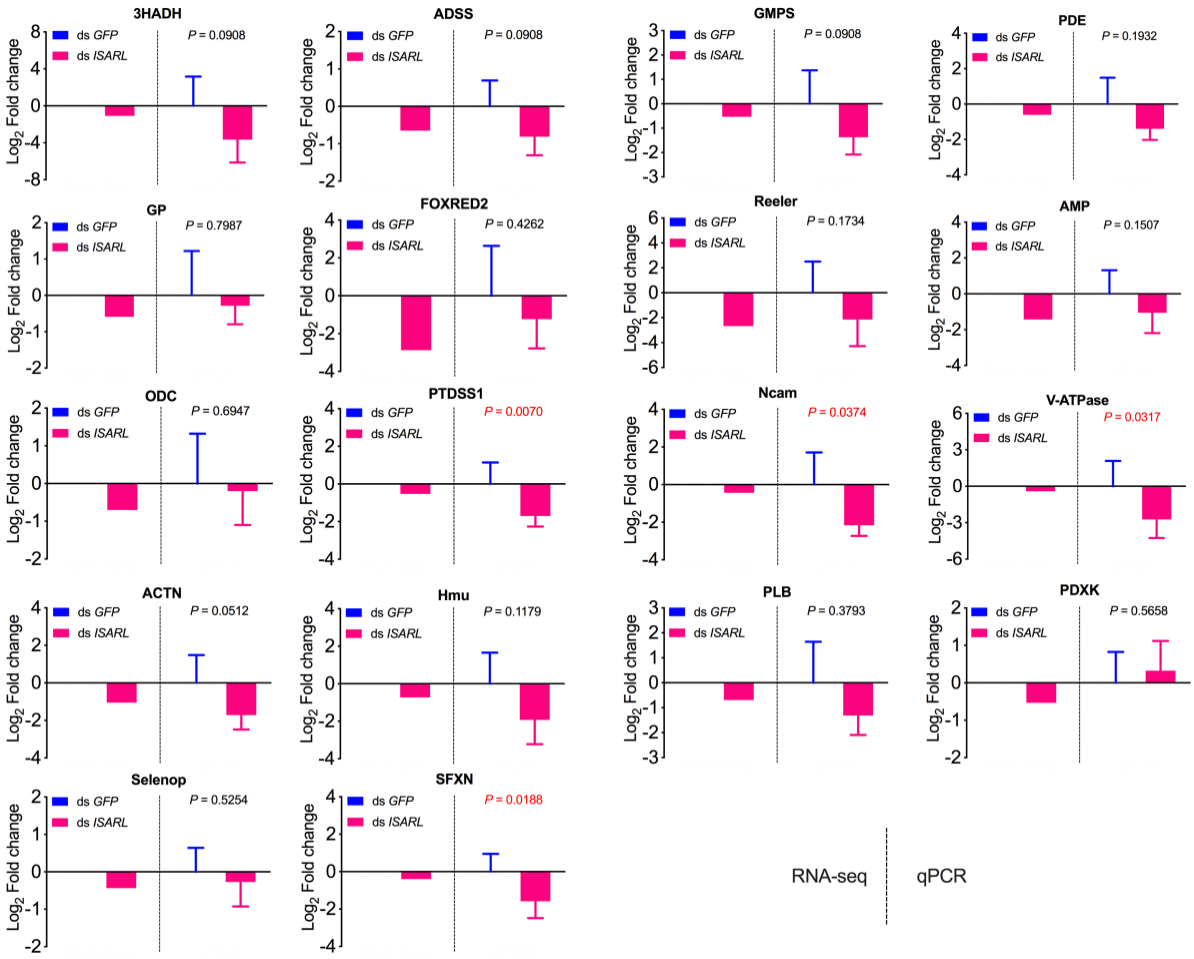

Figure S3. QPCR validation of 18 well-annotated and metabolism-related differentially expressed genes. 3HADH, 3-hydroxyacyl-CoA dehydrogenase, putative; ADSS, Adenylosuccinate synthetase; GMPS, GMP synthase, putative; PDE, cAMP and cAMP-inhibited cGMP 3,5-cyclic phosphodiesterase; GP, glycogen phosphorylase; FOXRED2, FAD dependent oxidoreductase domain-containing protein 2; Reeler, Secreted protein with Reeler domain; AMP, AMP dependent CoA ligase; ODC, Oxodicarboxylate carrier protein; PTDSS1, Phosphatidylserine synthase I; Ncam, N-CAM Ig domain-containing protein; V-ATPase, vacuolar H+-ATPase V1 sector, subunit G; ACTN, Alpha-actinin, putative; Hmu, Hemomucin, putative; PLB, Phospholipase B-like;

PDXK, Pyridoxine kinase, putative; Selenop, selenoprotein P precursor; SFXN, sideroflexin 1,2,3, putative.

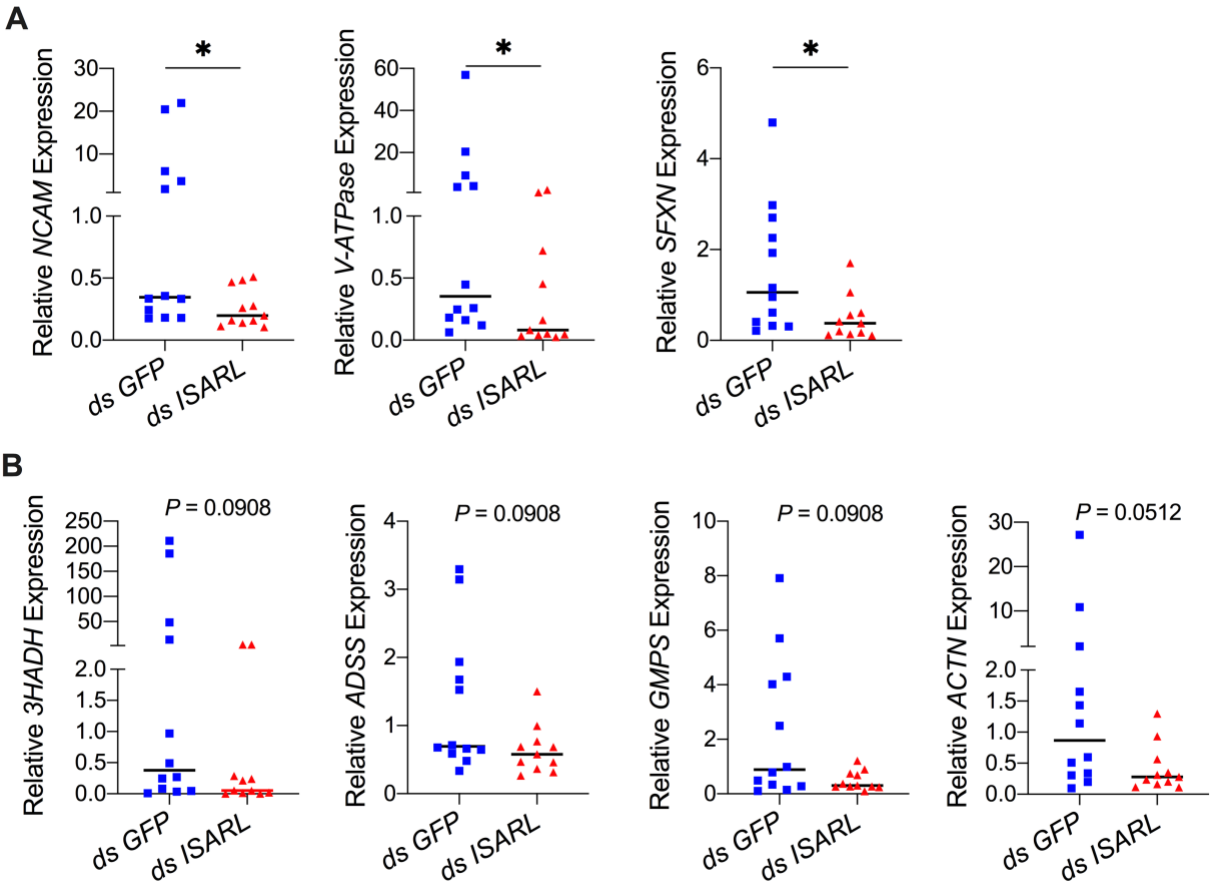

Figure S4. QPCR validation of differentially expressed genes from the RNA-seq dataset. (A) N-CAM Ig domain-containing protein (*NCAM*), Vacuolar H+-ATPase V1 sector, subunit G (*V-ATPase*), and Sideroflexin 1,2,3, putative (*SFXN*) were significantly downregulated following RNAi silencing of *ISARL* after feeding on *B. burgdorferi*-infected mice. (B) 3-hydroxyacyl-CoA dehydrogenase, putative (*3HADH*), Adenylosuccinate synthetase (*ADSS*), GMP synthase, putative (*GMPS*), and Alpha-actinin, putative (*ACTN*) were downregulated following RNAi silencing of *ISARL* after feeding on *B. burgdorferi*-infected mice (*P*-values are close to significant of 0.05). Each data point represents one nymph gut. Horizontal bars in the above figures represent the median. Statistical significance was assessed using a non-parametric Mann-Whitney test (*, $P < 0.05$).

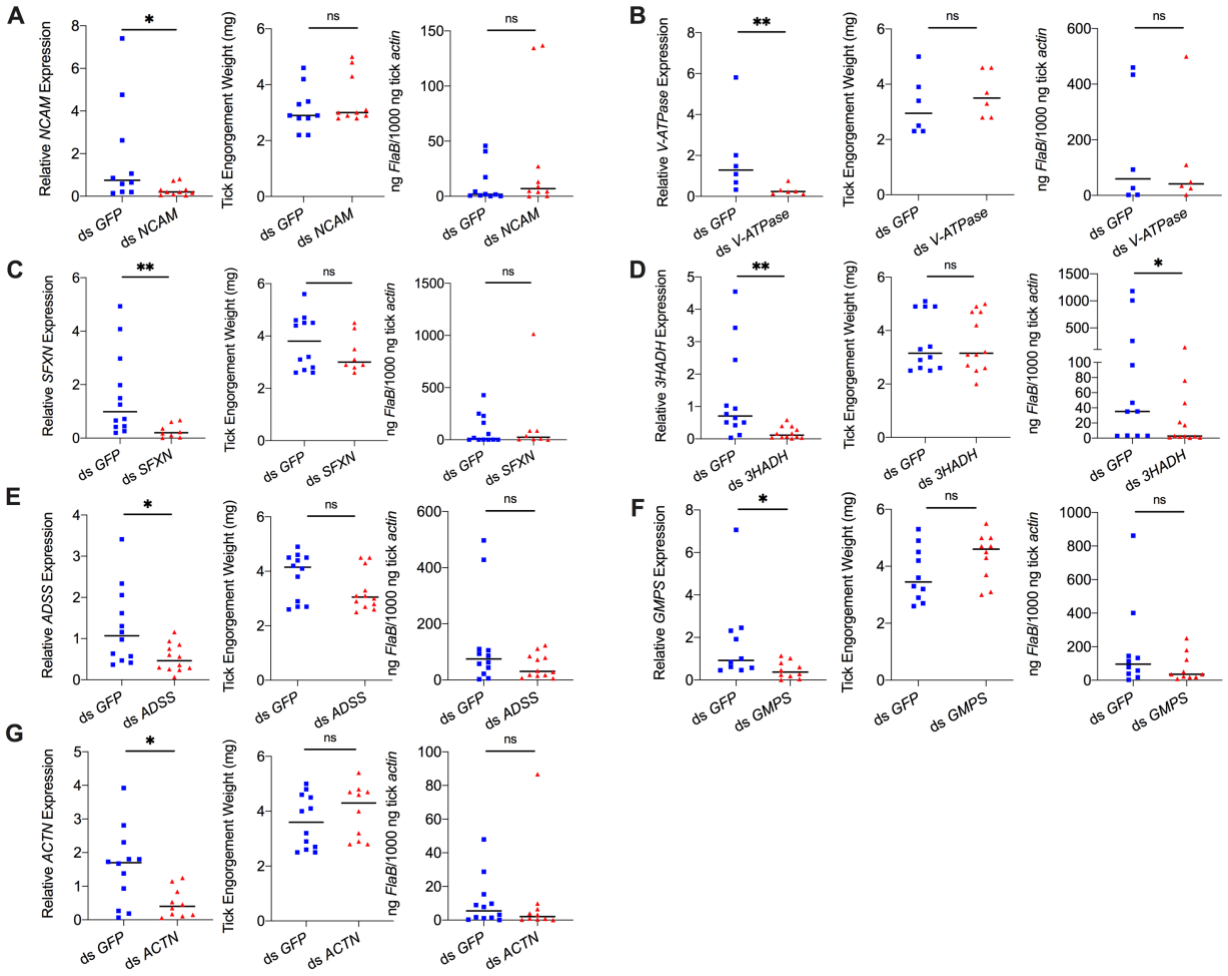

Figure S5. Silencing of differentially expressed genes and effects on *B. burgdorferi* acquisition. Silencing of (A) *NCAM*, (B) *V-ATPase*, (C) *SFXN*, (E) *ADSS*, (F) *GMPS*, and (G) *ACTN* has no effect on *B. burgdorferi* acquisition. Silencing of (D) *3HADH* decreased the *B. burgdorferi* burden in tick gut. 3HADH is involved in fatty acid metabolic processes, suggesting that tick fatty acid metabolism may also influence acquisition of *B. burgdorferi*. 3HADH is not significantly regulated by ISARL, it was not considered further in this study. Each data point represents one nymph gut. Horizontal bars in the above figures represent the median. Statistical significance was assessed using a non-parametric Mann-Whitney test (ns, $P > 0.05$; *, $P < 0.05$; **, $P < 0.01$).

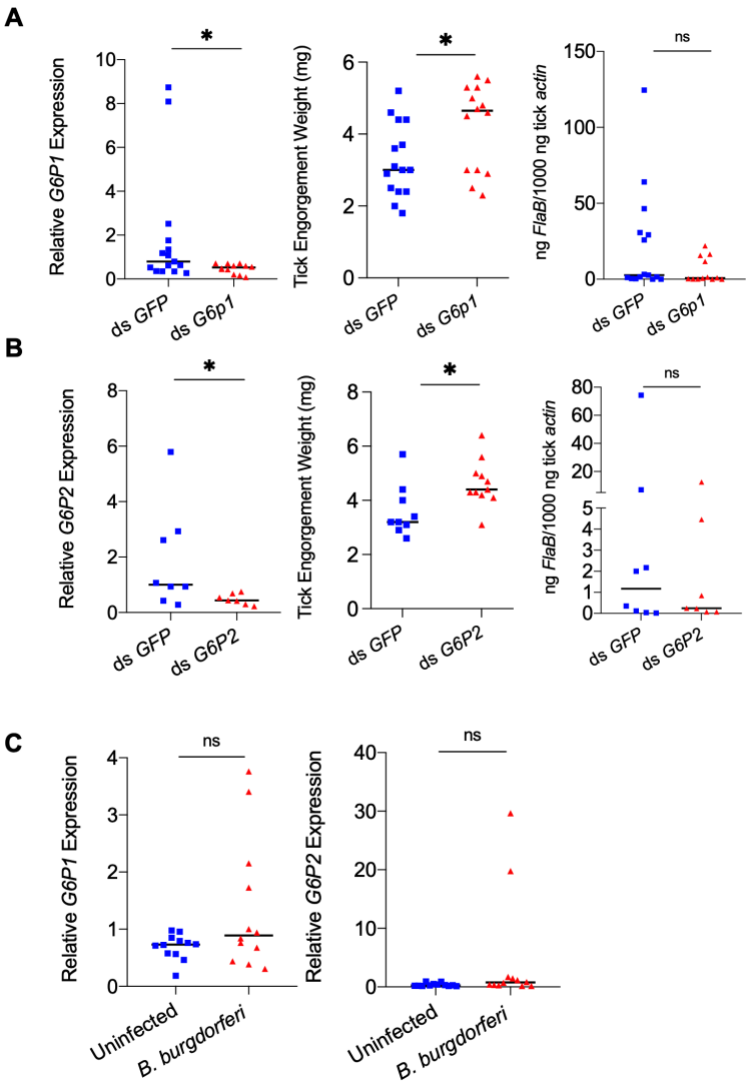

Figure S6. Mammalian adiponectin and tick glucose metabolism changes have no effect on *B. burgdorferi* acquisition. (A) qPCR assessment of *G6P1* transcript level, nymphal engorgement weights, and qPCR assessment of *B. burgdorferi flaB* levels in guts following RNAi silencing of *G6P1* after feeding on *B. burgdorferi*-infected mice. (B) qPCR assessment of *G6P2* transcript level, nymphal engorgement weights, and qPCR assessment of *B. burgdorferi flaB* levels in guts following RNAi silencing of *G6P2* after feeding on *B. burgdorferi*-infected mice. (C) qPCR assessment of *G6P1* and *G6P2*

transcript level in nymphal tick gut after feeding on clean and *B. burgdorferi*-infected mice (ns, $P > 0.05$; *, $P < 0.05$).

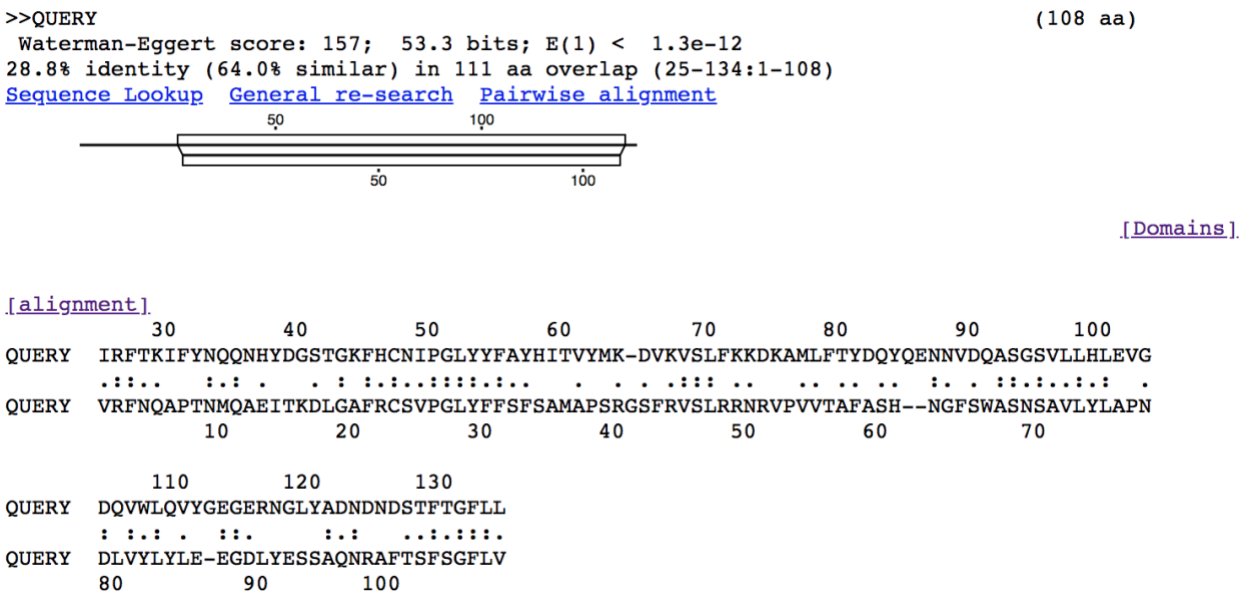

Figure S7. Alignment of human adiponectin C1Q domain and C1QL3 C1Q domain.

Tick C1QL3 C1Q domain has 64.0% similarity and 28.8% identity with human adiponectin C1Q domain. The alignment was conducted in LALIGN/PLALIGN (https://fasta.bioch.virginia.edu/fasta_www2/fasta_www.cgi?rm=lalign&pgm=lal).

Table S1. Summary of differently expressed genes of comparison between ds *GFP* and ds *ISARL* injection after 96h feeding on clean mice.

Gene	Annotation	Gene Name	GO function	Log2FoldChange	P-value
ISCW003049-RA	Soluble maltase-glucoamylase, putative (Fragment)	MGA	carbohydrate metabolic process	6.956779911	3.80E-06
ISCW007360-RA	Gamma glutamyl transpeptidase, putative	GGT	glutathione catabolic process	6.22827548	5.26E-07
ISCW024014-RA	Gamma glutamyl transpeptidase, putative (Fragment)	GGT	glutathione catabolic process	6.190152254	5.27E-06
ISCW024661-RA	Gamma glutamyl transpeptidase, putative (Fragment)	GGT	glutathione catabolic process	6.190152254	5.27E-06
ISCW012872-RA	Gamma-glutamyltransferase, putative (Fragment)	GGT	glutathione catabolic process	6.012757202	2.94E-11
ISCW009571-RA	Uncharacterized protein (Fragment)	ISCW009571	N/A	3.298128524	2.41E-05
ISCW024915-RA	REX4, RNA exonuclease 4 (S. cerevisiae) family protein (Fragment)	REX4	nucleic acid binding	-0.549991457	2.24E-05
ISCW024422-RA	Superoxide dismutase, putative	SOD	removal of superoxide radicals	-1.11031654	5.27E-05
ISCW012336-RA	Superoxide dismutase [cu-zn], putative	CuZnSOD	removal of superoxide radicals	-1.117657247	3.62E-05
ISCW005879-RA	Uncharacterized protein	ISCW005879	N/A	-1.608105744	1.35E-05
ISCW012069-RA	Uncharacterized protein	ISCW012069	N/A	-1.810228584	2.52E-06
ISCW009622-RA	Uncharacterized protein	ISCW009622	N/A	-2.535341888	1.26E-06
ISCW018477-RA	Adiponectin receptor, putative (Fragment)	ISARL	adiponectin-activated signaling pathway	-2.75905145	3.57E-22
ISCW003837-RA	G2/mitotic-specific cyclin A, putative (Fragment)	cyclinA	mitotic cell cycle phase transition; regulation of cyclin-dependent protein serine/threonine kinase activity	-3.145555868	1.43E-06
ISCW002566-RA	Acyl-CoA synthetase, putative (Fragment)	ACS	acetate-CoA ligase activity	-3.53392918	5.23E-05

ISCW008490-RA	Gamma glutamyl transpeptidase, putative	GGT	glutathione catabolic process	-5.476120094	5.66E-08
ISCW013319-RA	Uncharacterized protein	ISCW013319	N/A	-7.608882724	2.05E-07
ISCW009608-RA	Glutathione S-transferase, putative	GST	glutathione metabolic process	-7.655953275	1.37E-05

"-" indicates downregulation of genes in the guts of ds *ISARL*-injected ticks when compared to that in control ds *GFP*-injected tick guts.

Table S2. Summary of differently expressed genes of comparison between ds *GFP* and ds *ISARL* injection after 96h feeding on *B. burgdorferi*-infected mice.

Gene	Annotation	Gene Name	GO function	Log2FoldChange	P-value
ISCW003218-RA	FADdependent oxidoreductase domain-containing protein 2, putative	FOXRED2	ubiquitin-dependent ERAD pathway	-2.879056472	0.000239
ISCW005667-RA	Secreted protein, putative	Reeler	N/A	-2.678543731	0.000119
ISCW003629-RA	Secreted protein, putative	ISCW003629	N/A	-2.426582135	0.0001
ISCW018477-RA	Adiponectin receptor, putative (Fragment)	ISARL	adiponectin-activated signaling pathway	-1.912092255	1.72E-11
ISCW011292-RA	Cyclic nucleotidebinding domain-containing protein	CNBD	potassium ion transmembrane transport	-1.620397316	0.00021
ISCW003135-RA	Cytochrome p450, putative	CYP	heme binding; oxidoreductase activity	-1.427275425	7.35E-05
ISCW001955-RA	AMP dependent CoA ligase, putative	AMP	oxidoreductase activity	-1.427082757	0.00027
ISCW002185-RA	Uncharacterized protein	ISCW002185	N/A	-1.251407193	3.40E-05
ISCW024631-RA	3-hydroxyacyl-CoA dehydrogenase, putative (Secreted salivary gland peptide, putative)	3HADH	fatty acid metabolic process	-1.089854316	2.66E-05
ISCW013566-RA	Alpha-actinin, putative	ACTN	calcium ion binding; protein tyrosine phosphatase activity	-1.051823169	4.99E-05
ISCW020505-RA	Uncharacterized protein	ISCW020505	oxidoreductase activity	-1.038498406	4.11E-05
ISCW019656-RA	Secreted salivary gland peptide, putative (Fragment)	ISCW019656	N/A	-1.000151879	5.89E-05
ISCW016391-RA	Cytochrome P450, putative	CYP	heme binding; oxidoreductase activity	-0.983747879	0.000348
ISCW006151-RA	Transport protein, putative (Fragment)	ISCW006151	transmembrane transporter activity	-0.869973215	1.75E-05
ISCW021203-RA	Uncharacterized protein	ISCW021203	N/A	-0.826491344	9.19E-05

ISCW024161-RA	Uncharacterized protein	ISCW024161	N/A	-0.753881171	4.99E-05
ISCW018609-RA	Hemomucin, putative (Fragment)	Hmu	biosynthetic process	-0.730567529	0.000361
ISCW017282-RA	Oxodicarboxylate carrier protein, putative	ODC	transmembrane transport	-0.701243498	4.69E-05
ISCW009471-RA	Phospholipase B-like (Fragment)	PLB	phospholipid catabolic process	-0.694463465	8.01E-05
ISCW006150-RA	Sugar transporter, putative	ISCW006150	carbohydrate transport	-0.666272429	6.70E-05
ISCW012299-RA	Adenylosuccinate synthetase (Fragment)	ADSS	de novo' AMP biosynthetic process; IMP metabolic process	-0.649923076	0.00038
ISCW022913-RA	cAMP and cAMP-inhibited cGMP 3,5-cyclic phosphodiesterase, putative	PDE	negative regulation of cGMP-mediated signaling	-0.612276289	3.11E-06
ISCW000885-RA	Alpha-1,4 glucan phosphorylase	GP	glycogen catabolic process	-0.588614232	0.000254
ISCW019117-RA	Pyridoxine kinase, putative (Fragment)	PDXK	pyridoxal 5'-phosphate salvage	-0.535676385	0.000478
ISCW018543-RA	GMP synthase, putative (Fragment)	GMPS	glutamine metabolic process; GMP biosynthetic process	-0.53194689	0.000465
ISCW004028-RA	Phosphatidylserine synthase I, putative	PTDSS1	phosphatidylserine biosynthetic process	-0.529598437	3.12E-05
ISCW012521-RA	Uncharacterized protein	ISCW012521	N/A	-0.517853294	2.92E-05
ISCW009548-RA	Uncharacterized protein	ISCW009548	N/A	-0.504914087	0.000199
ISCW015732-RA	RNA polymerase II transcription elongation factor, putative	Elongin-C	ubiquitin-dependent protein catabolic process	-0.48942716	4.89E-05
ISCW022144-RA	N-CAM Ig domain-containing protein, putative	Ncam	protein serine phosphatase activity; protein threonine phosphatase activity	-0.437192969	0.000289

ISCW009549-RA	Selenoprotein P precursor, putative	Selenop	selenium compound metabolic process	-0.436460074	0.000423
ISCW013692-RA	V-type proton ATPase subunit G	V-ATPase	proton transmembrane transport	-0.414399839	0.000311
ISCW010157-RA	Receptor expression-enhancing protein	REEP	N/A	-0.405156446	0.000104
ISCW023312-RA	Sidoreflexin	SFXN	mitochondrial transmembrane transport; serine import into mitochondrion	-0.3999554	0.000229
ISCW006433-RA	AP complex subunit sigma (Fragment)	APS	intracellular protein transport; vesicle-mediated transport	-0.395796427	0.000508

"-" indicates downregulation of genes in the guts of ds *ISARL*-injected ticks when compared to that in control ds *GFP*-injected tick guts.

Table S3. Summary of differently expressed genes of comparison between recombinant *GFP* and adiponectin proteins injection after 8h.

Gene	Annotation	Log2FoldChange	*P*-value
ISCW004553-RA	Cuticle protein, putative	18.51302808	2.05E-12
ISCW002039-RA	Cuticle protein, putative	17.49563794	2.29E-07
ISCW001782-RA	Uncharacterized protein	17.27754175	7.09E-10
ISCW013798-RA	Cuticle protein, putative	17.20315541	7.96E-05
ISCW015495-RA	Secreted protein, putative (Fragment)	17.15463748	0.00016026
ISCW005191-RA	Secreted glycine rich protein, putative (Fragment)	17.11093994	2.95E-08
ISCW003789-RA	Uncharacterized protein	16.81877212	2.70E-06
ISCW016297-RA	Uncharacterized protein	16.74612219	1.13E-06
ISCW008562-RA	Cuticle protein, putative	15.3237752	1.02E-06
ISCW002925-RA	Uncharacterized protein	2.857394251	1.82E-05
ISCW024478-RA	Secreted cysteine rich protein, putative (Fragment)	2.851254132	1.38E-05
ISCW021558-RA	Secreted salivary gland peptide, putative	2.689268024	3.51E-05
ISCW021555-RA	Uncharacterized protein	2.656702948	4.30E-05
ISCW023547-RA	Secreted salivary gland peptide, putative	2.589439049	0.0001213
ISCW023623-RA	Serpin-4 precursor, putative (Serpin-4, putative)	2.173997552	5.42E-05
ISCW008209-RA	Hebreain, putative	2.158930697	1.20E-06
ISCW024733-RA	Beat protein, putative (Fragment)	2.105356324	1.12E-05
ISCW024387-RA	Serpin-2 precursor, putative (Fragment)	2.00955178	5.56E-05
ISCW002113-RA	Antimicrobial peptide microplusin	1.940836315	0.00014064
ISCW011893-RA	ANK_REP_REGION domain-containing protein	1.808330643	1.28E-08

ISCW015113-RA	Uncharacterized protein	1.783621042	6.95E-05
ISCW012685-RA	Myosin light chain 1, putative	1.61605594	9.51E-05
ISCW005837-RA	Uncharacterized protein	1.582477028	3.43E-05
ISCW024686-RA	Ixoderin, putative (Fragment)	1.545371762	3.67E-06
ISCW014652-RA	Serpin-8 precursor, putative	1.431124914	1.89E-06
ISCW009063-RA	Tropomyosin, putative	1.358977546	0.00014404
ISCW023442-RA	Uncharacterized protein	1.288696108	0.00015793
ISCW023441-RA	Troponin, putative (Fragment)	1.2703018	0.00010777
ISCW016762-RA	LIM domain-containing protein, putative	1.268776381	6.91E-06
ISCW002637-RA	Reductase, putative	1.195839092	5.26E-05
ISCW017459-RA	Glucose-6-phosphatase	-1.182920138	0.00012321
ISCW015064-RA	Cytochrome P450, putative	-1.276584666	5.75E-06
ISCW015956-RA	Serine/threonine protein kinase, putative	-1.438675023	1.25E-05
ISCW016390-RA	Cytochrome P450, putative	-1.643963635	3.32E-06
ISCW016391-RA	Cytochrome P450, putative	-1.678990788	6.27E-05
ISCW006560-RA	Cytochrome P450, putative	-2.209859052	1.42E-06
ISCW024348-RA	Salivary HBP family protein, putative (Fragment)	-3.822772331	2.76E-05
ISCW008563-RA	Cuticle protein, putative	-14.56782308	1.01E-06
ISCW005940-RA	Elongation of very long chain fatty acids protein	-15.77527062	7.81E-08
ISCW012372-RA	Cysteine rich secreted peptide, putative	-17.69968417	3.20E-09

"-" indicates downregulation of genes in the guts of adiponectin-injected ticks when compared to that in control GFP-injected tick guts.

Table S4. The primers used in this study.

Gene name	Primer sequence
Tick *actin*	F: GGCGACGTAGCAG R: GGTATCGTGCTCGACTC
Mouse *β-actin*	F: AGCGGGAAATCGTGCGTG R: CAGGGTACATGGTGGTGCC
Borrelia flaB	F: TTCAATCAGGTAACGGCACA R: GACGCRRGAGACCCTGAAAG
ds *GFP*	F: *TAATACGACTCACTATAGGGAGA*GCGACGTAAACGGCCACAAGT T R: *TAATACGACTCACTATAGGGAGA*CGGGTCTTGTAGTTGCCGTC
ds *ISARL*	F: *TAATACGACTCACTATAGGGAGA*GACGATGACGAGGATGAGC R: *TAATACGACTCACTATAGGGAGA*CGTGTGGAAGGTGAAGGAC
ISARL qPCR	F: TGCAGGACAACGACTACCTG R: ACCAGATGTTCCCGGTCTC
*ISARL*_pEZT_Dlux	F: AGGCGTTCAGTCTAGAATGGAGGTCCGCGAGCGACG R: AGACCGGCGGCCGCTCAAGCGTAATCTGGAACATCGTATGGGTAGTCGAATGGTGGACCCTCCT
3HADH qPCR	F: GACCCCCTGATTGTTATTCG R: GCCATCCACTTCTTTCTTGA
ADSS qPCR	F: CACCGAGCAGAAGAACGAG R: GAGTAGCGGAGAACCACCAG
GMPS qPCR	F: CACCTTCATCACCCAGGACT R: TCTCGCTCACCATCTTCTTG
FOXRED2 qPCR	F: CCATCAACAACGACCTCTT R: GGCGTCCTAACTATCTTCAGT
Reeler qPCR	F: CCTGGAGGAACCTGAAGAAG R: AATGGCGTGGACGAAGTAAT
AMP qPCR	F: TACCACAACAAGCCACAAGC R: CGATGTAGAACTGCCCACTC
ODC qPCR	F: GTCTCACGGAGGCTGTCTTC R: TACGTGCTACGGCAAAGGTA
PDE qPCR	F: GACGGTGCGAAAGAACTACC R: TTGAATGCTCCTGTGGAATG
GP qPCR	F: GTGGAGATGCGAGAGGAGAT R: GTAGTCCCAGGCGTTGTAGC
PTDSS1 qPCR	F: ATGGCTTCGGCATCTTCTT R: TCGTGGTCTGAATGTCCTTG
Ncam qPCR	F: GCTGCGGGAGAACTATGTG R: CTTGTTGAGGTGTTGCTGCT
VATPase qPCR	F: ATGGCTAGTCAAAGCCAAGG R: CATCGGCGACTTTTTCAGAC

ACTN qPCR	F: ACCGCTACACCCAGTACACC R: TCTCGACCTCGTTGATGTTG
HMU qPCR	F: TCGACGCTTACTACGGTGTC R: GTCGTCCAGAAAGAGGATGC
PLB qPCR	F: GAATTTTCTCTGGCGACGAC R: AAGAGTTGCCGTTCCCTGT
PDXK qPCR	F: CTGAAAGAGGACAACCCTTCA R: GCTCCCTGTAGATGCTCACC
Selenop qPCR	F: CAGTGCAAGAAACTCCACCA R: AAAGTCTGGACGCCTTCGTA
SFXN qPCR	F: TCTCTGCGGTCTTCTGCTC R: CGAACCACCTCCTGAATCTC
ds *3HADH*	F: *TAATACGACTCACTATAGGGAGA*GTTGCACTCTTTGACGTGGA R: *TAATACGACTCACTATAGGGAGA*AGTGGGACGTAGTATGGTGGA
ds *PTDSS1*	F: *TAATACGACTCACTATAGGGAGA*CTAGTCAAAAGCCCGACCAC R: *TAATACGACTCACTATAGGGAGA*TGACCGCATACTCCTTCTCA
ds *ADSS*	F: *TAATACGACTCACTATAGGGAGA*CAGTGGTGAACAGCGTGAA R: *TAATACGACTCACTATAGGGAGA*TTGGTGGAAGTCAAAAACGA
ds *GMPS*	F: *TAATACGACTCACTATAGGGAGA*AAGGACTTCCACAAGGACGA R: *TAATACGACTCACTATAGGGAGA*ACACGTACACCACCCTGTTG
ds *NCAM*	F: *TAATACGACTCACTATAGGGAGA*ACTTTGGAGGTGCTGGACA R: *TAATACGACTCACTATAGGGAGA*AGAGAGTGGCAGACGGAGAC
ds *ACTN*	F: *TAATACGACTCACTATAGGGAGA*ATCTGCTGGACTACGGGAAG R: *TAATACGACTCACTATAGGGAGA*GGGTGTTGAAGTTGGTCTCC
ds *SFXN*	F: *TAATACGACTCACTATAGGGAGA*TTGGGACCAGAGCACCTACT R: *TAATACGACTCACTATAGGGAGA*GAAGCGTCCTACCAGAGGAG
ds *V-ATPase*	F: *TAATACGACTCACTATAGGGAGA*GAAGCAGGCAAAGGATGAAG R: *TAATACGACTCACTATAGGGAGA*AACGTCAGGAGCTGCTCAAT
ds *PSD*	F: *TAATACGACTCACTATAGGGAGA*GACTACCACCGCTTCCACTC R: *TAATACGACTCACTATAGGGAGA*CCTCGAAGATGAGCACCAC
PSD qPCR	F: GAAGGGCATCACCTACTCC R: CTTCTGCTGGTACTCCTCCTC
G6P1 qPCR	F: AGCCTGTCCCGAATCTACA R: CGTTGTCCGTGTCCATCTT
G6P2 qPCR	F: TCCATCTATTTCGGGCTGAT R: GTTCACGTAGGTCGGGTCAT
PEPCK1 qPCR	F: CAACACCATTTTCACCAACG R: AGTTTGCCTCCCTTTTCCA
PEPCK2 qPCR	F: TTCCACTGCCCAAGTATCG R: GCTCCGTGCTGATGAATGT
PEPCK3 qPCR	F: GAGCACAAAGGCAAGGTGA R: TTCCCAGACTCAGCCAATG

ds *G6P1*	F: *TAATACGACTCACTATAGGGAGA*GCCAGTGCTATGTCCACCT R: *TAATACGACTCACTATAGGGAGA*GAGACGCCCCGATAAAGAC
ds *G6P2*	F: *TAATACGACTCACTATAGGGAGA*AGCACCGACCCTTCTGGTA R: *TAATACGACTCACTATAGGGAGA*GATGACCCCACTGACTACGG
ds *C1QL3*	F: *TAATACGACTCACTATAGGGAGA*GAACATGCAGGCAGAAATCA R: *TAATACGACTCACTATAGGGAGA*ACGAGAAAGCCCGAGAAAG
C1QL3 qPCR	F: ACGAGAGCCATCACCTCCT R: TCCCCTTTCTGCGAATAAGA
C1QL3_pMT	F: CTCGCTCGGGAGATCTATGCAGACCTGGGTTGTTCTTG R: GCCCTCTAGACTCGAGTACCGTCCCCTTTCTGCGAAT

The underlines indicate restriction enzymes sites. The italicized letters indicate T7 promoter sequence.